Actin scaffolding by clathrin heavy chain is required for skeletal muscle sarcomere organization

Stéphane Vassilopoulos,[1,2,3,4] Christel Gentil,[1,2,3,4] Jeanne Lainé,[1,2,3,4,5] Pierre-Olivier Buclez,[1,2,3,4,7] Agathe Franck,[1,2,3,4] Arnaud Ferry,[1,2,3,4,6] Guillaume Précigout,[1,2,3,4,7] Robyn Roth,[8] John E. Heuser,[8] Frances M. Brodsky,[9] Luis Garcia,[1,2,3,4,7] Gisèle Bonne,[1,2,3,4] Thomas Voit,[1,2,3,4] France Piétri-Rouxel,[1,2,3,4] and Marc Bitoun[1,2,3,4]

[1]Institut National de la Santé et de la Recherche Médicale (INSERM) U974, [2]Centre National de la Recherche Scientifique (CNRS) UMR 7215, and [3]Université Pierre et Marie Curie–Paris 6, UM 76, Paris F-75013, France
[4]Institut de Myologie, Paris F-75013, France
[5]Département de Physiologie, Université Pierre et Marie Curie–Paris 6, Site Pitié-Salpêtrière, Paris F-75013, France
[6]Université Paris Descartes–Paris 5, 75006 Paris, France
[7]Université de Versailles – Saint-Quentin-en-Yvelines, 78000 Versailles, France
[8]Department of Cell Biology and Physiology, Washington University, St. Louis, MO 63110
[9]Departments of Bioengineering and Therapeutic Sciences, Pharmaceutical Chemistry, and Microbiology and Immunology, University of California, San Francisco, San Francisco, CA 94143

The ubiquitous clathrin heavy chain (CHC), the main component of clathrin-coated vesicles, is well characterized for its role in intracellular membrane traffic and endocytosis from the plasma membrane (PM). Here, we demonstrate that in skeletal muscle CHC regulates the formation and maintenance of PM–sarcomere attachment sites also known as costameres. We show that clathrin forms large coated lattices associated with actin filaments and the muscle-specific isoform of α-actinin at the PM of differentiated myotubes. Depletion of CHC in myotubes induced a loss of actin and α-actinin sarcomeric organization, whereas CHC depletion in vivo induced a loss of contractile force due to the detachment of sarcomeres from the PM. Our results suggest that CHC contributes to the formation and maintenance of the contractile apparatus through interactions with costameric proteins and highlight an unconventional role for CHC in skeletal muscle that may be relevant to pathophysiology of neuromuscular disorders.

Introduction

Clathrin is composed of trimerized heavy chains (CHCs) with bound light chains (CLCs) and assembles to form a membrane coat. The clathrin lattice formation on cellular membranes is initiated by clathrin adaptors that are drawn into the lattice and trigger clathrin-coated vesicle (CCV) budding at various subcellular compartments (Pearse and Robinson, 1990; Kirchhausen, 1999; Brodsky, 2012). Once the invagination process has initiated, dynamin family members associate with the neck of the forming pit, recruit additional proteins including actin, and allow the scission of the coated vesicle (Fujimoto et al., 2000; Merrifield et al., 2002). The role of dynamin 2 (DNM2) in skeletal muscle has received considerable attention because the

autosomal-dominant form of centronuclear myopathy (CNM) has been linked to mutations in the *DNM2* gene (Bitoun et al., 2005). DNM2 is involved in various cellular processes, but to date it remains unclear whether its role in CCV fission is implicated in centronuclear myopathy.

Several recent studies have proposed a role for clathrin and dynamin in actin organization that is distinct from coated vesicle formation (Schafer et al., 2002; Veiga et al., 2007; Saffarian et al., 2009; Bonazzi et al., 2011, 2012). Intriguingly, a role for clathrin in myofibril assembly was previously proposed (Kaufman et al., 1990), and several teams have reported direct protein–protein interaction between CHC, α-actinin, and vinculin, two focal adhesion proteins crucial for muscle function (Schook et al., 1979; Burridge et al., 1980; Merisko, 1985;

The Rockefeller University Press $30.00
J. Cell Biol. Vol. 205 No. 3 377–393
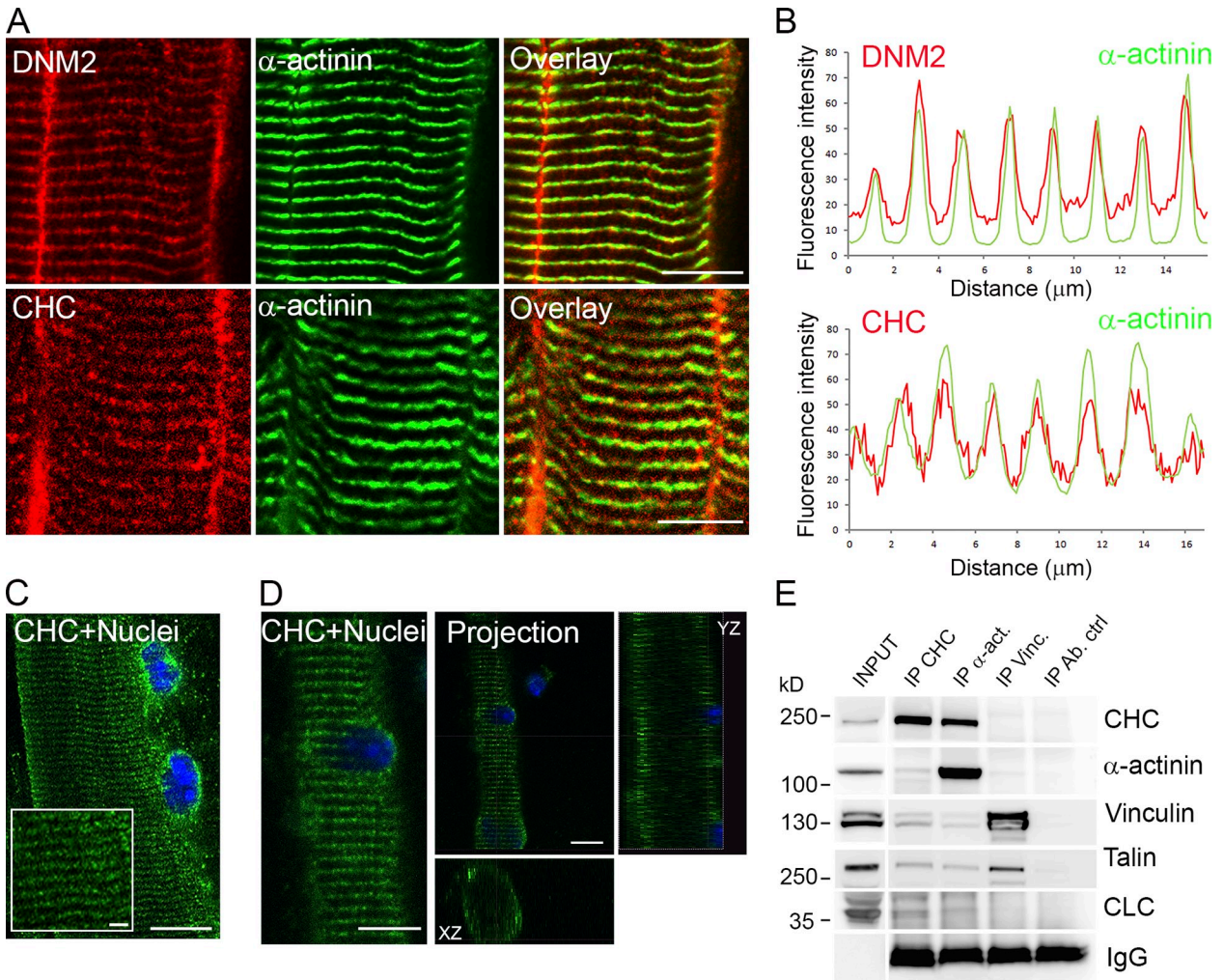www.jcb.org/cgi/doi/10.1083/jcb.201309096

JCB 377

Figure 1. **CHC association with α-actinin2 in adult skeletal muscle.** (A) Confocal sections of mouse skeletal muscle were processed for double-immuno-fluorescent labeling of DNM2 (red) and α-actinin (green) or CHC (red) and α-actinin (green). Bars, 10 µm. (B) The fluorescence intensity as a function of distance on the fiber was plotted for eight successive striations, and was reported on the graph for each labeling. The green curve corresponds to the green immunolabeling, and the red curve corresponds to the red labeling. (C and D) CHC localization in mouse dissociated FDB fibers. (C) Confocal sections of fibers processed for immunofluorescent labeling with the monoclonal antibody against CHC (X22, green). Bars: (main panel) 10 µm; (inset) 2 µm. (D) XZ and YZ projections of confocal optical sections illustrated in C. Bars, 10 µm. (E) Immunoblot of proteins associated with CHC, α-actinin (isoform 2), vinculin, or control immunoprecipitates from mouse muscle lysates and 1–5% lysate input. Bands for coimmunoprecipitated CHC, α-actinin (isoform 2), vinculin, talin, or CLC are indicated at the right.

Merisko et al., 1988; Fausser et al., 1993). α-Actinin and vinculin are expressed in both skeletal and cardiac muscles, where they are localized to a specialized compartment called the "costamere."

Costameres, muscle-specific adhesion sites, are sub-sarcolemmal protein assemblies circumferentially aligned in register with Z-disks of peripheral myofibrils. They were originally described as electron-dense plaques rich in the focal adhesion protein vinculin, and function as attachment complexes (Pardo et al., 1983a,b; Shear and Bloch, 1985). They are located between the plasma membrane and myofibrils and play both a mechanical and a signaling role during contraction, transmitting force from the contractile apparatus to the ECM in order to stabilize skeletal muscle fibers. They are considered as the "Achilles' Heel" of skeletal muscle because, when disrupted, they directly contribute to the development of several distinct myopathies (Blake et al., 2002; Ervasti, 2003). In the present work, we have addressed the role played by CHC in skeletal

muscle costamerogenesis and costamere maintenance. We show that clathrin associates with α-actinin at the surface of myotubes and forms large plaques that are associated with actin filaments. Depletion of CHC induces severe defects in α-actinin distribution and subsequently leads to defective costamere formation in vitro and induces impairment of contractile properties associated with structural abnormalities including sarcomere disorganization as well as detachment of the sarcomeres from the sarcolemma in vivo.

Results

CHC is a component of the costameric complex in skeletal muscle

In adult skeletal muscle, DNM2 and CHC are both localized at the level of the I-band and present a striated pattern that overlaps with the muscle-specific α-actinin (isoform 2) staining
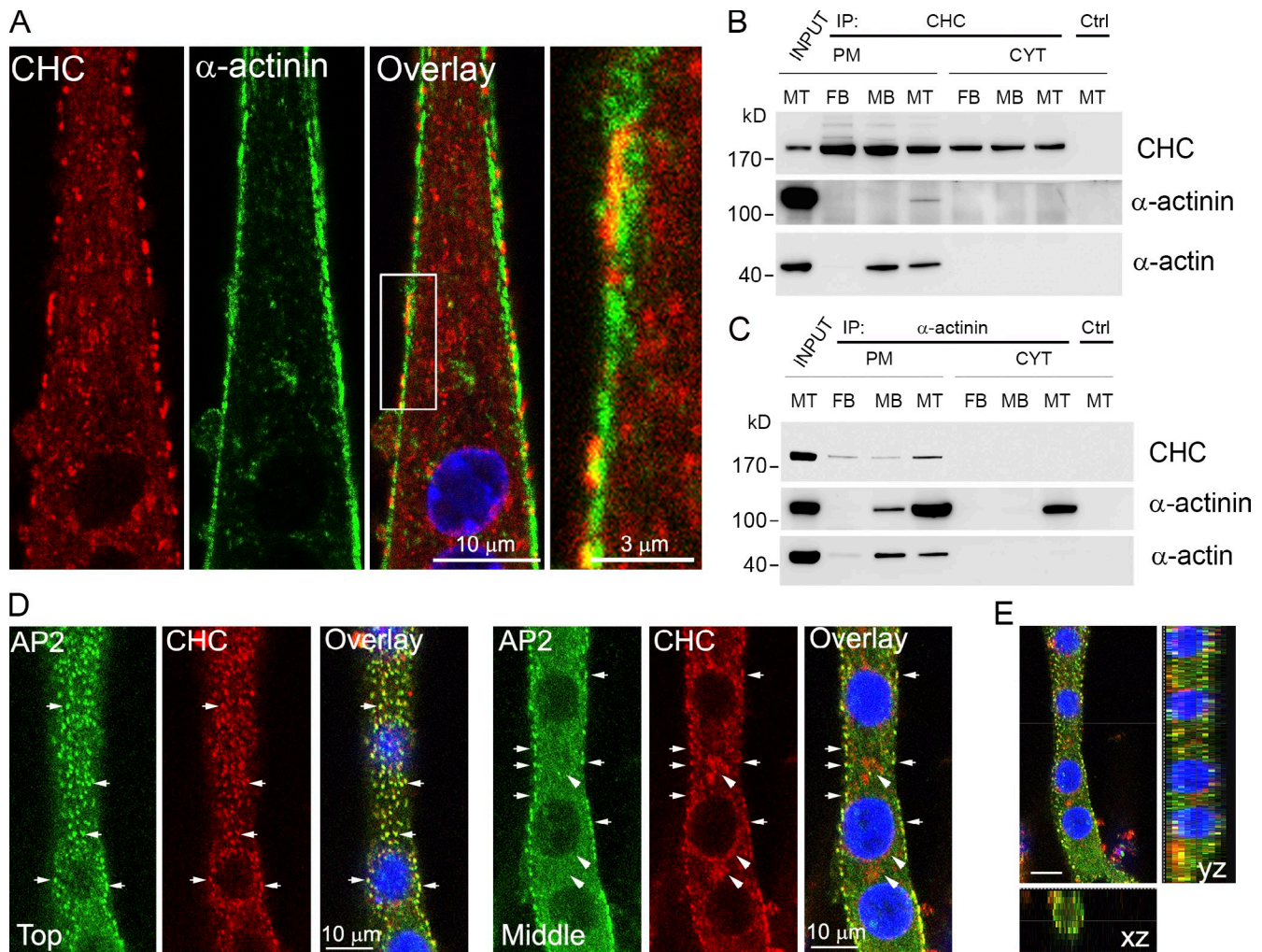
Figure 2. **CHC association with α-actinin2 and actin at the PM of differentiated myotubes.** (A) Localization of α-actinin (green) and CHC (red) in mouse primary myotubes differentiated for 4 d. Inset in Overlay panel is displayed on the right. (B) Immunoblot analysis of proteins associated with CHC or control immunoprecipitates from subcellular fractions (plasma membrane, PM and cytosol, CYT) of 3T3 fibroblasts (FB), undifferentiated C2C12 (MB), and differentiated C2C12 cells (MT). (C) Immunoblot analysis of proteins associated with α-actinin or control immunoprecipitates from subcellular fractions (PM and CYT) of 3T3 fibroblasts (FB), undifferentiated C2C12 (MB), and differentiated C2C12 cells (MT). (D) Confocal microscopy of AP2 (green) and CHC (red) in differentiated C2C12 skeletal muscle cells. The left panel displays images from the top of the myotube and the right panel displays images from the middle of the myotube. Arrows indicate large clusters of colocalization between AP2 and CHC and arrowheads indicate intracellular clusters near the nuclei positive for CHC and negative for AP2. (E) XZ and YZ projections of serial confocal sections are shown on the overlay. Bar, 10 μm.

(Fig. 1, A and B; Kaufman et al., 1990; Butler et al., 1997; Towler et al., 2004; Durieux et al., 2010; Cowling et al., 2011). Using confocal optical sectioning and 3D reconstruction, we demonstrated that this striated labeling was mainly present at the surface of dissociated fibers (Fig. 1, C and D). Analysis of the compartment labeled by anti-CHC antibodies on adult skeletal muscle using electron microscopy revealed that clathrin is present along the sarcolemma and localizes at sites that correspond to contacts between sarcolemma and Z-discs, which are also densely stained with tannic acid (Fig. S1, A and B). As several studies have described a direct association between α-actinin and vinculin with clathrin (Schook et al., 1979; Burridge et al., 1980; Merisko, 1985; Merisko et al., 1988; Fausser et al., 1993), we then assessed the association between clathrin and the α-actinin–vinculin–talin complex in adult mouse skeletal muscle (Fig. 1 E). We observed coimmunoprecipitation of CHC and CLC upon α-actinin immunoprecipitation, but only minor

amounts of vinculin and talin. Additionally, minor amounts of α-actinin are detected upon clathrin immunoprecipitation while vinculin coimmunoprecipitates talin efficiently and some α-actinin, but not clathrin. This suggests that part of the α-actinin pool is associated with clathrin in a complex distinct from the vinculin–talin–α-actinin complex.

We further characterized the sites of interaction between CHC and α-actinin during the early steps of differentiation in primary myotubes and showed that these proteins partially colocalize along the plasma membrane (PM) after 4 d of differentiation (Fig. 2 A). By subcellular fractionation, we observed an association between α-actinin and CHC in the PM fraction of fibroblasts, myoblasts, and differentiated myotubes. This association was stronger in differentiated myotubes as the levels of α-actinin expression increase (Fig. 2, B and C). In addition, we detected α-actin in both CHC and α-actinin immunoprecipitates from muscle cells. Several adaptor proteins are required
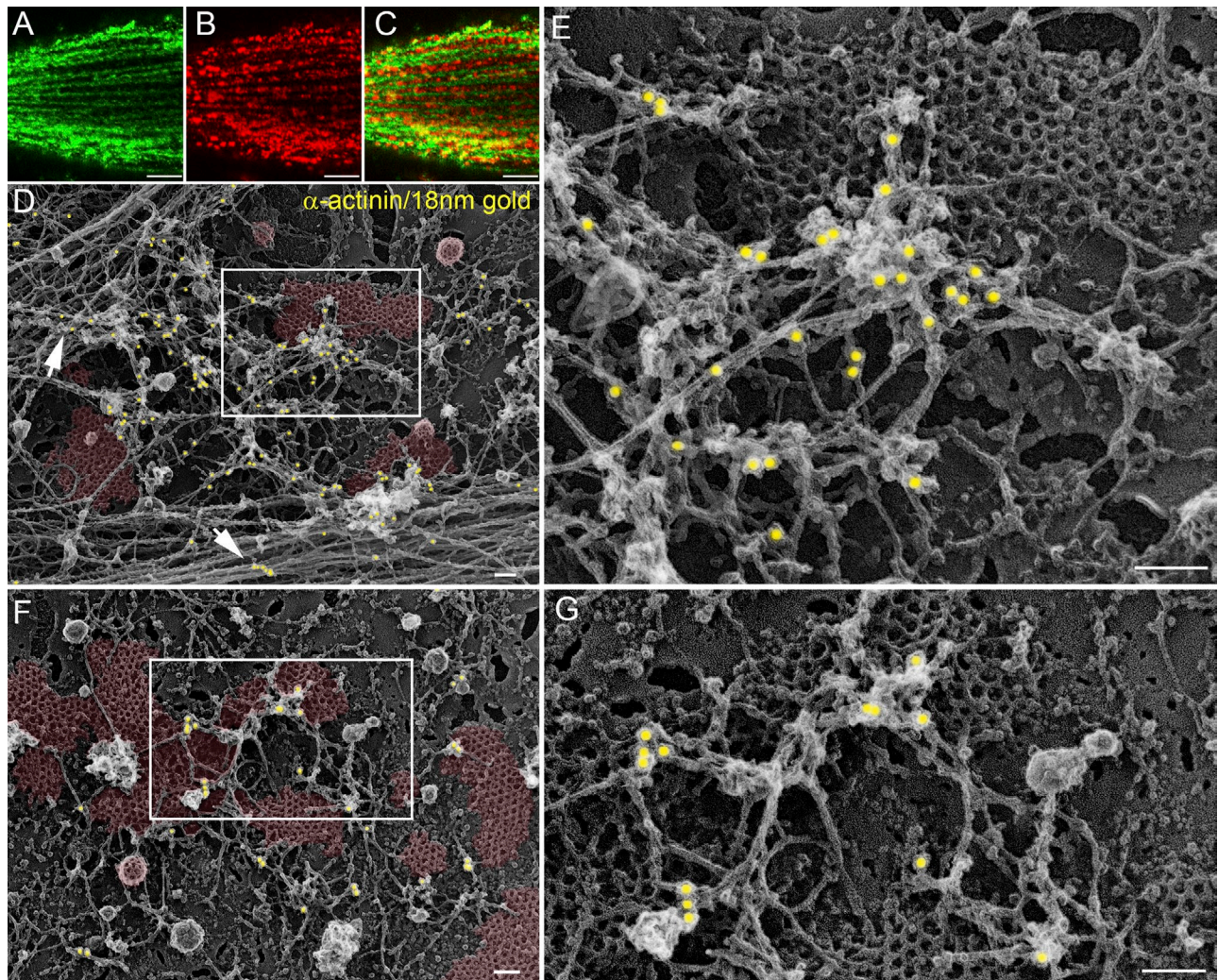
Figure 3. **α-Actinin and actin are localized on large flat clathrin-coated plaques.** (A–C) Immunofluorescent staining of α-actinin (A), CHC (B), and merged images (C) in untreated differentiated primary mouse myotubes visualized using confocal microscopy. Bars, 5 µm. (D–G) Adherent plasmalemmal sheets prepared from control primary myotubes differentiated for 4 d and labeled with α-actinin antibodies followed by secondary antibodies conjugated to 18-nm colloidal gold particles. Gold particles are pseudocolored yellow (D–G) and clathrin lattices are pseudocolored pale red (D and F). The boxed region in D and F is magnified in E and G, respectively. Note that α-actinin is found on both actin cables (D, arrows) and branched filaments lying on top of flat clathrin-coated lattices. Bars, 100 nm.

for targeting clathrin to specific intracellular compartments and, among these, AP2 is involved in recruiting clathrin to the PM. In differentiated myotubes, AP2 was localized at the surface of myotubes and displayed a predominant PM localization (Fig. 2, D and E). These results show that clathrin is a costameric protein that is recruited by AP2 and associates with actin and α-actinin at the PM of differentiated myotubes.

Costameric clathrin forms large plaques where α-actinin and actin are localized

Myofibril assembly and subsequent sarcomere formation initiate at the PM. After the formation of a subcortical actin lattice, additional nascent sarcomeres keep adding to the initial actin network (Dlugosz et al., 1984; Epstein and Fischman, 1991; Sanger et al., 2002; Quach and Rando, 2006). We hypothesized that α-actinin and actin rely on a clathrin scaffold at the PM to start recruiting additional myofibrils and explored this possibility using immunogold cytochemistry coupled with quick-freeze,

deep-etch rotary replication and electron microscopy (Heuser, 1980). We showed that clathrin forms two distinct coated structures, i.e., large plaques that contain much more polymerized clathrin that would be required to form a single vesicle (pseudo-colored in red in Fig. 3, D and F) and coated vesicles found in regions devoid of plaques (Fig. 3, D and F; and Fig. S1, C–G). Using clathrin antibodies we were able to confirm that CHC was indeed the proteinaceous material composing these structures (Fig. S1, C–K). As expected, α-actinin strongly labeled dense longitudinally organized actin filament bundles (Fig. 3 D, arrows; and Fig. S2, A and B) that are reminiscent of the contractile apparatus. In addition, α-actinin was associated with actin filaments that surround or overlap flat clathrin lattices (Fig. 3, E and G; and Fig. S2, A, C, and D) highly enriched with the adhesion marker β5 integrin (Fig. S2, E–H) as previously described on rat myotubes (De Deyne et al., 1998; Pumplin, 1989; Pumplin and Bloch, 1990), whereas vinculin was not localized at these clathrin-coated plaques (unpublished data).
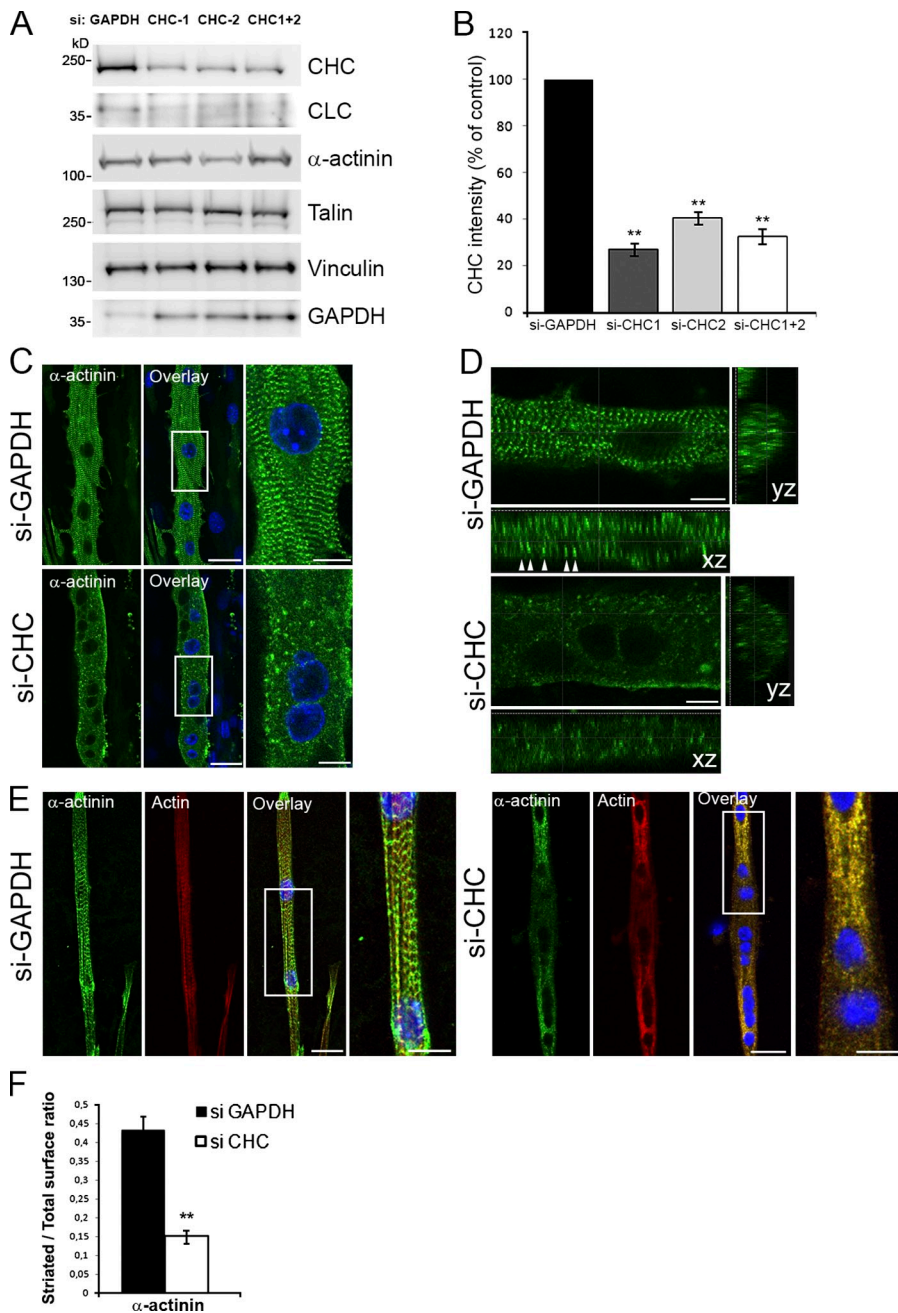
Figure 4. **CHC regulates formation and organization of sarcomeres in cultured myotubes.** (A) Differentiated C2C12 cells were treated with control GAPDH siRNA, two different siRNA targeting CHC, a mixture of both (CHC-1, CHC-2, CHC-1+2 indicated at the top), and cell lysates immunoblotted for proteins (indicated at the right). (B) CHC expression in cultured C2C12 myotubes treated with GAPDH or CHC siRNA. The graph depicts quantification of CHC band intensity ($n = 8$ for CHC-1 and $n = 4$ for CHC-2 and CHC1+2; data are presented as mean ± SEM; **, $P < 0.01$). (C) α-Actinin staining in differentiated C2C12 skeletal muscle cells treated with control GAPDH siRNA or CHC siRNA. DNA staining (DAPI blue) identifies multinucleated myotubes. The boxed region in the merged images is magnified in the insets. Bars: (main panels) 30 µm; (insets) 10 µm. (D) XZ and YZ projections of serial confocal sections. Bars, 10 µm. (E) CHC depletion on cultured primary mouse myotubes. Immunofluorescent staining of α-actinin (green) and actin (red) in differentiated primary mouse myotubes treated with control GAPDH siRNA or CHC siRNA. DNA staining (DAPI blue) identifies differentiated, multinucleated myotubes. The boxed region in the merged images is magnified in the insets. Bars: (main panels) 20 µm; (insets) 10 µm. (F) Quantification of striated vs. nonstriated surface in control (siRNA against GAPDH) or in myotubes treated with siRNA against CHC ($n = 30$–60 myotubes, data are presented as mean ± SEM; **, $P < 0.01$).

Our experiments on primary myotubes show that CHC forms large plaques that may serve to anchor the actin cytoskeleton and α-actinin.

CHC is required for the formation of costameres

We next tested the effect of CHC knockdown on α-actinin subcellular organization. We achieved high knockdown efficiency in C2C12 myotubes differentiated for 6 d (Fig. 4, A and B) with two previously published siRNA sequences (Ezratty et al., 2009). Additionally, we showed that levels of CLC were also reduced because of the instability of the light chain upon heavy chain depletion, as previously reported in nonmuscle cells (Brodsky, 1985; Esk et al., 2010). Expression levels of α-actinin, vinculin, and talin were unaffected in myotubes treated with CHC siRNA (Fig. 4 A).

As expected, control myotubes present a striated α-actinin distribution after 6 d of differentiation. This striated pattern is first visible at the periphery of the myotube and gradually fills the entire cytoplasm (Quach and Rando, 2006). In CHC-depleted myotubes, the α-actinin striated pattern was strongly disrupted, and instead, clusters of α-actinin were randomly dispersed in the intracellular space (Fig. 4 C). 3D projections of confocal sections confirmed a dramatic reduction of the striated pattern between controls and CHC-depleted myotubes (Fig. 4 D). Upon CHC depletion, a similar phenotype arises in mouse primary myotubes (Fig. 4, E and F) in which organization of actin filaments is also affected. To determine the role played by clathrin during the early steps of costamere formation, we performed siRNA depletion experiments on C2C12 myotubes after 4 d of differentiation, before α-actinin and actin could reach a striated organization. In control myotubes, α-actinin

Figure 5. **CHC, AP2, and DNM2 but not AP1 or AP3 depletion in cultured mouse myotubes perturbs α-actinin distribution before striations appear.** (A) Differentiated C2C12 myotubes were treated with siRNA targeting proteins (indicated at the left). Immunofluorescent staining of α-actinin in myotubes treated with control siRNA against GAPDH or siRNA targeting either CHC, AP1, AP2, AP3, or DNM2. DNA staining (DAPI blue) identifies differentiated, multinucleated myotubes. The boxed region in the merged images is magnified in the insets. Bars: (main panels) 10 μm; (insets) 5 μm. (B) Quantification of α-actinin fluorescence surface as a function of total myotube surface in 4-d differentiated myotubes treated with siRNA against GAPDH, CHC, AP1, AP2, AP3, or DNM2 (n = 30–50 myotubes, data are presented as mean ± SEM; **, P < 0.01).
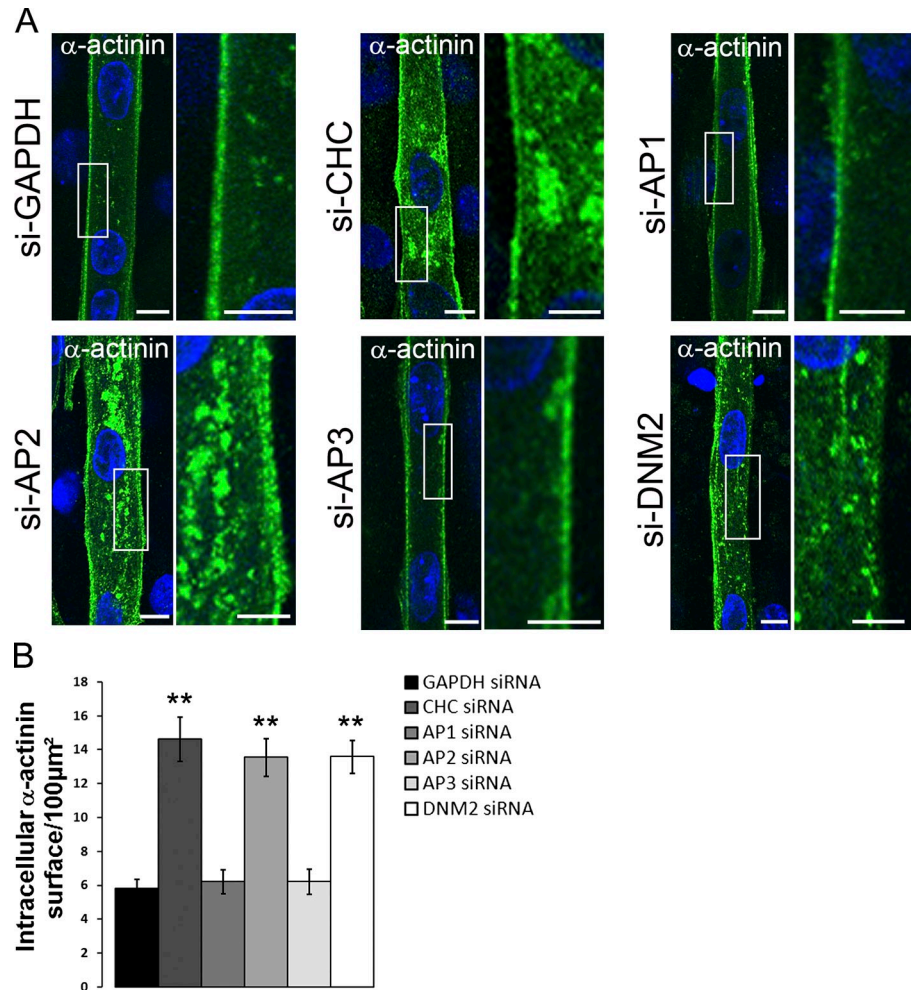
was mainly localized along the PM. In stark contrast, myotubes that had been depleted of CHC presented a strong increase in the amount of intracellular α-actinin (Fig. 5 A). These results demonstrate that CHC is required for proper α-actinin distribution during early myotube differentiation.

AP2 and DNM2 are required for α-actinin scaffold formation

We next tested the effect of AP2 knockdown on α-actinin subcellular localization. AP2 (α-subunit) depletion by siRNA (Fig. S3 C) induced a strong decrease in the amount of CHC recruited at the PM. More importantly, AP2 knockdown phenocopied the effect of CHC depletion on α-actinin distribution and dramatically increased the intracellular α-actinin staining (Fig. 5). We have also depleted the AP1 (γ-subunit) and AP3 (δ-subunit) adaptors responsible for CHC targeting at the Golgi apparatus and endosomal systems. As expected, AP1 and AP3 were localized at the perinuclear region and in intracellular structures dispersed throughout the myotube (Fig. S3 A). siRNA depletion of AP1 and AP3 drastically reduced the intracellular CHC staining without affecting CHC localization at the PM (unpublished data). Moreover, knockdown of AP1 and AP3 had no effect on α-actinin distribution (Fig. 5), suggesting that the impact of CHC depletion on α-actinin organization is

not due to perturbations of the secretory pathway or trafficking between the endo/lysosomal system.

DNM2 is also present at or near the plasma membrane of differentiating myotubes, where its staining partially overlaps with that of α-actinin (Fig. S4 C). AP2 depletion strongly reduced the amount of DNM2 at the plasma membrane, suggesting that part of the PM staining corresponds to an association with clathrin lattices (Fig. S4 D). Efficient DNM2 depletion (Fig. S3 A) induced an increase in the amount of intracellular α-actinin staining (Fig. 5 and Fig. S4 A). Of interest, these intracellular aggregates observed upon CHC, AP2, and DNM2 depletion also contain actin aggregates (Fig. S4 A).

We performed the quantification of the intracellular α-actinin–positive area for all siRNA constructs (Fig. 5 B). CHC, AP2, and DNM2 had a strong impact on the intracellular α-actinin area, whereas AP1 and AP3 values were not different from controls. Altogether, these results confirm that the primary impact observed upon CHC depletion on α-actinin organization is related to its cytoskeleton scaffolding role at the PM through a process also involving AP2 and DNM2.

Hip1R depletion stabilizes α-actinin and actin on clathrin-coated structures

Actin has been shown to be present at CCVs (Collins et al., 2011), and a requirement for actin has been suggested for clathrin
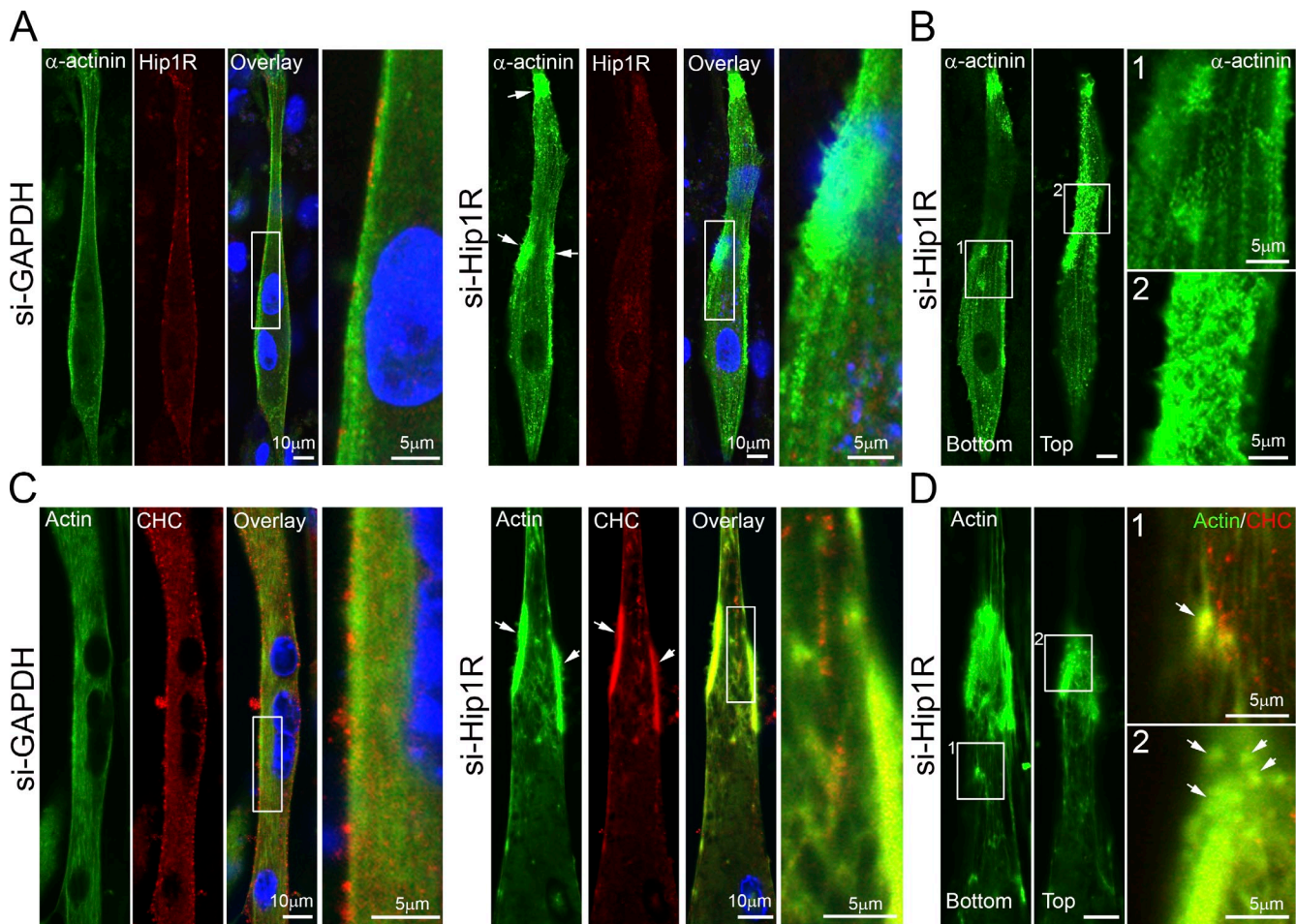
Figure 6. **Hip1R depletion in cultured myotubes stabilizes actin and α-actinin on clathrin-coated structures.** (A) Immunofluorescent staining of α-actinin (green) and Hip1R (red) in differentiated C2C12 myotubes treated with control siRNA against GAPDH or siRNA targeting Hip1R. DNA staining (DAPI blue) identifies differentiated, multinucleated myotubes. The boxed region in the merged images is magnified in the insets. Bars: (main panels) 10 µm; (insets) 5 µm. (B) α-Actinin localization in differentiated C2C12 skeletal muscle cells treated with siRNA targeting Hip1R. The left panel displays an image from the bottom of the myotube and the right panel displays an image from the top of the myotube. The boxed regions in the images are magnified in the insets 1 and 2. Bars: (main panels) 10 µm; (insets) 5 µm. (C) Immunofluorescent staining of actin and CHC in myotubes treated with control siRNA against GAPDH or siRNA targeting Hip1R. DNA staining (DAPI blue) identifies differentiated, multinucleated myotubes. The boxed region in the merged images is magnified in the insets. Bars: (main panels) 10 µm; (insets) 5 µm. (D) Actin localization in differentiated C2C12 skeletal muscle cells treated with siRNA targeting Hip1R. The left panel displays an image from the bottom of the myotube and the right panel displays an image from the top of the myotube. The boxed regions in the images are magnified in the insets (1 and 2) and include CHC staining (red). Bars: (main panels) 10 µm; (insets) 5 µm. Arrows in A, C, and D indicate large peripheral clusters of α-actinin or actin and CHC.

plaque formation (Saffarian et al., 2009). Interaction between actin and clathrin is mediated by Hip1R (huntingtin-interacting protein 1–related protein) and CLC (Engqvist-Goldstein et al., 2001, 2004; Chen and Brodsky, 2005; Legendre-Guillemin et al., 2005; Brodsky, 2012). In myotubes, Hip1R colocalizes with AP2-positive puncta in differentiated myotubes (Fig. S3 D). We tested the effect of both CHC and AP2 depletion on Hip1R (Fig. S3 D) and showed a dramatic reduction of the Hip1R staining at the PM. These results confirm that CHC and AP2 are required for recruiting the clathrin-associated actin-binding protein Hip1R to the PM. It has been shown that Hip1R depletion stabilizes the actin filaments on clathrin-coated plaques in HeLa cells (Engqvist-Goldstein et al., 2004). We decided to test the contribution of Hip1R on the distribution of actin and α-actinin in differentiated myotubes. siRNA depletion of Hip1R drastically reduced Hip1R protein levels (Fig. S3 A). Hip1R-depleted myotubes had a disorganized actin cytoskeleton and α-actinin distribution. The

Hip1R-depleted myotubes accumulated unusual actin structures near the cell cortex (Fig. 6). These structures, which are very similar to the ones observed by Engqvist-Goldstein et al. (2004) upon Hip1R depletion in HeLa cells, took a variety of forms, including tails and rings at the bottom and the top of differentiated myotubes (Fig. 6 and Fig. S4 B). These results demonstrate that when Hip1R expression is reduced, actin polymerization at clathrin-coated structures is no longer properly regulated and results in accumulation of actin and α-actinin on clathrin-coated plaques.

CHC is required for sarcomere maintenance in mature isolated muscle fibers

We then assessed the function of CHC in mature skeletal muscle fibers. For this purpose, we developed an AAV strategy combined with the use of a short hairpin RNA (shRNA) against CHC (AAV-shCHC) for ex vivo transduction of isolated fibers

Figure 7. **CHC is required for sarcomere maintenance in adult fibers.** (A) Quantitative RT-PCR and (B) Western blot analysis of CHC levels and proteins indicated at the right in FDB fibers infected with AAV-CTRL or AAV-shCHC for 12 d in vitro. (C) Quantification of Western blot CHC band intensity ($n = 3$, data are presented as mean ± SEM; for A and C: **, $P < 0.01$). (D–G) Confocal microscopy of dissociated FDB fibers infected with AAV-CTRL or AAV-shCHC for 12 d and co-stained with antibodies against either α-actinin and CHC (D), α-actinin and DNM2 (E), or F-actin (phalloidin staining) and caveolin-3 (F and G). All bars, 10 µm.
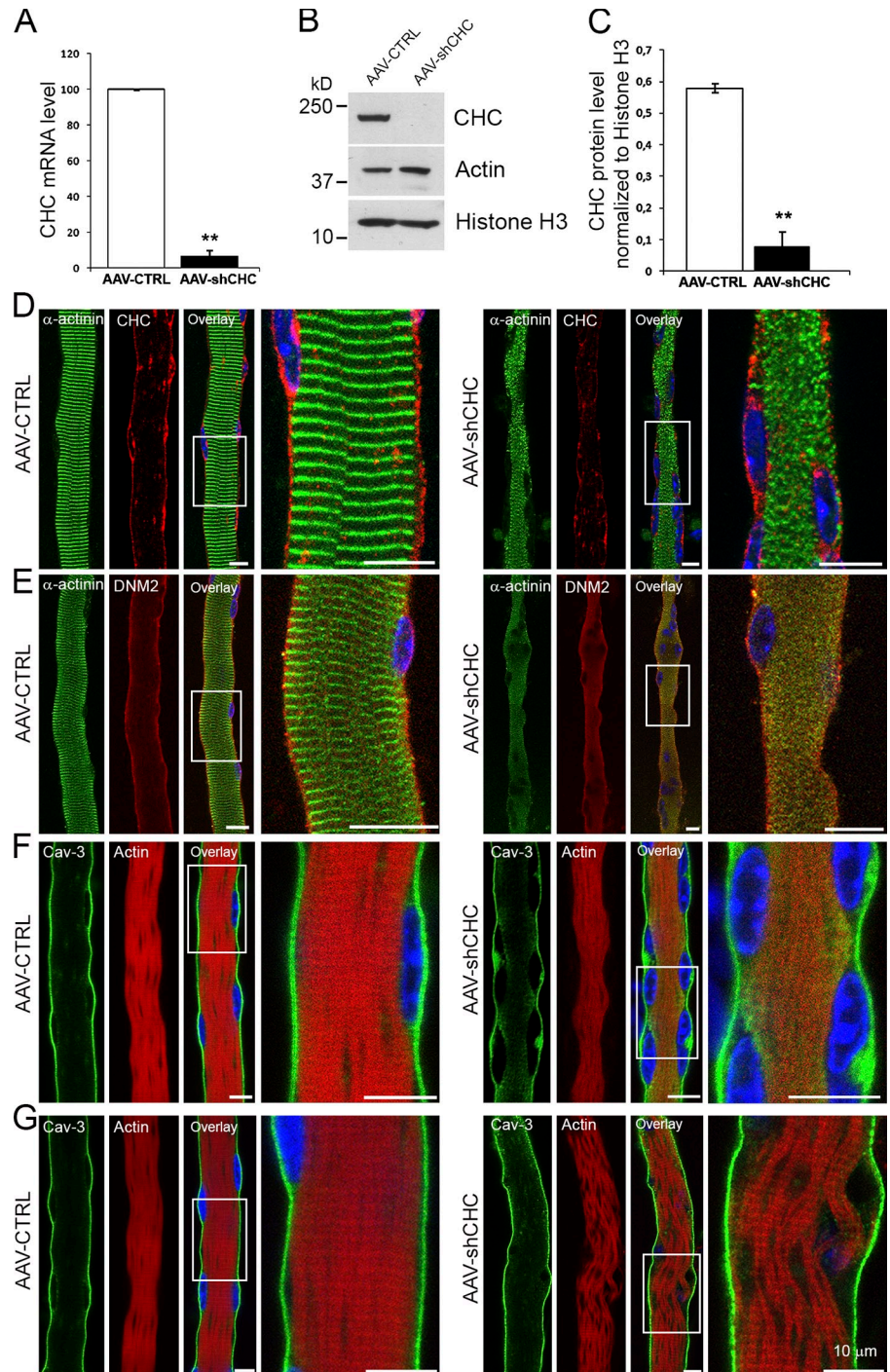
from flexor digitorum brevis (FDB) muscle. In AAV-shCHC–infected fibers, a strong decrease in CHC expression was confirmed, both at the RNA and protein level (Fig. 7, A–C), and α-actinin was no longer correctly localized, with very few striations noticeable and displaying a diffuse or disorganized staining pattern (Fig. 7 D). We also tested the effect of CHC depletion on DNM2 distribution. In control fibers, DNM2 displayed a striated pattern at the surface, with each striation being centered on the I-band, and in the core of the fiber DNM2 was mainly present at the PM (Durieux et al., 2010; Cowling et al.,

2011). In fibers depleted of CHC, the DNM2 signal at the core of the fiber was greatly reduced at the PM (Fig. 7 E). To assess the effect of CHC depletion on the integrity of the actin cytoskeleton we used phalloidin staining. In control fibers, F-actin displayed a regularly spaced striated distribution. However, CHC-depleted fibers presented a diffuse actin distribution (Fig. 7 F), and in some fibers detachment of entire sarcomeric bundles (Fig. 7 G). In addition to its role in costamerogenesis, these data suggest that CHC is also involved in their preservation in mature fibers.

In vivo CHC depletion impairs force and causes muscle degeneration

We used AAV-shCHC in order to induce an in vivo depletion of CHC in tibialis anterior (TA) muscle. By performing hematoxylin and eosin staining on transverse TA sections (Fig. 8 A), no histological change was visible in muscles injected with control AAV or with AAV-shCHC until day 18 post-injection (PI). However, fibers displaying a rounded shape with a clearly disorganized intracellular space were noticed at day 21 PI. Between days 21 and 23 PI some degenerating fibers appeared, and by day 25 PI the vast majority of the fibers had a rounded shape with a clear degenerating phenotype. As a general feature of muscle degeneration, an immune infiltration was visible at day 21 and was extremely pronounced by days 23 and 25 PI. At day 25, small myotubes appeared and their presence reached a peak by day 38 where the majority of the muscle was centrally nucleated, the signature of a muscle undergoing massive regeneration.

Quantitative RT-PCR and Western blot analysis confirmed that at day 18 PI a strong decrease in CHC had indeed occurred (Fig. 8, B–D). When we measured CHC RNA and protein levels at later time points, we noticed that CHC levels increased from 40% back to 55% of control levels at day 21 PI and were back to control levels by day 23. Surprisingly, at day 25 PI, CHC levels were higher in the AAV-shCHC–injected muscle compared with the contralateral control muscle (Fig. 8, B and C). A possible explanation is that the infiltration by macrophages contaminates our analysis with exogenous clathrin from nontransduced immune cells. Indeed, at days 21, 23, and 25 PI a strong increase in CD11b protein levels was evident (Fig. 8 C and Fig. S5, A and B). Immunofluorescent staining confirmed that CD11b-positive macrophages had massively infiltrated the CHC-depleted muscle. In fact, CD11b protein levels correlated perfectly with the sudden increase in CHC levels. To circumvent the immune infiltration and to show that a clathrin knockdown had occurred, we performed immunoprecipitation experiments using antibodies against the muscle-specific α-actinin isoform. This assay enabled us to show that in muscles injected with AAV-shCHC, there was a strong decrease in the amount of CHC which coimmunoprecipitated with α-actinin (Fig. 8 E).

Direct muscle stimulation was performed in order to measure the maximal isometric strength of the TA muscle in CHC-depleted muscles. At day 18 PI, when no morphological alteration could be observed, CHC depletion induced a 57% decrease in specific maximal force, i.e., absolute maximal force divided by muscle weight (Fig. 8 F). At day 21 PI, CHC depletion had an even more robust effect; muscle depleted of CHC displayed a 74% decrease in specific maximal force (Fig. 8 F). No significant muscle mass loss was observed at both early time-points (Fig. 8 G). These results show that AAV-shCHC efficiently knocks down CHC in vivo with dramatic consequences in terms of muscle fiber homeostasis.

In vivo CHC depletion perturbs α-actinin, γ-actin, and DNM2 distribution

We then sought to analyze the distribution of α-actinin, DNM2, and the costameric actin isoform γ-actin (Sonnemann et al., 2006) in CHC-depleted skeletal muscle by immunocytochemistry. At 18 d PI, the α-actinin labeling was not different from the control, whereas a clear reduction in sarcolemmal clathrin was apparent (Fig. 9 A). However, at day 21 and at further time points (day 23 and day 25), α-actinin and γ-actin both displayed a diffuse distribution compared with control muscle, and areas where α-actinin was no longer adjacent to the sarcolemma were also visible (Fig. 9, B–D). In addition, in control fibers DNM2 presented a strong PM staining and a weak intracellular staining. At day 21 and at further time points (day 23 and day 25) the DNM2 intracellular staining was greatly enhanced (Fig. 9, B and D). We also tested the effect of CHC depletion on the distribution of other costameric proteins such as dystrophin, β-dystroglycan, and caveolin-3 (Fig. S5, B and C). Even though at days 23 and 25 the muscle presented a severe dystrophic phenotype, no change in the distribution of these proteins was noticeable. We therefore conclude that CHC depletion has a strong effect on the localization of intracellular costameric proteins related to the actin cytoskeleton, including γ-actin, actin-associated proteins, and DNM2, without affecting the distribution of dystrophin and PM integral components such as members of the dystrophin-associated glycoprotein complex.

In vivo CHC depletion induces disorganization of the contractile apparatus and detachment between the sarcolemma and myofibrils

We performed electron microscopy analysis of CHC-depleted muscle at day 18 PI (without phenotype upon HE analysis) and at day 25 PI (peak of degeneration). At day 18 PI, focal regions displayed sarcomere abnormalities such as Z-band streaming and disorganization of the contractile apparatus especially in the I-band region (Fig. 10, A–C). It is of interest that these focal sarcomeric disorganizations were usually found adjoining the sarcolemma. In addition, at day 18 PI, occasional detachments of the sarcomeric apparatus from the sarcolemma were visible (Fig. 10, E–G). Both these phenotypes were consistent with the phenotypes produced upon clathrin depletion on isolated fibers. Of note, the T-tubule and sarcoplasmic reticulum system did not seem affected in the disorganized regions (Fig. 10 D). At day 25 PI, both transverse (Fig. 10, H–J) and longitudinal sections (Fig. 10, K and L) presented a particularly exacerbated detachment phenotype, with fibers displaying large areas of the sarcolemma that were no longer associated with sub-sarcolemmal sarcomeres.

Discussion

In this study, we identify a new role for CHC in costamere formation and maintenance. Our results raise the possibility that CHC, AP2, and DNM2 contribute to the formation of the costameric scaffold that is necessary for anchoring the actin cytoskeleton by recruitment of actin-binding protein Hip1R and actin cross-linking protein α-actinin early during myotube differentiation. Consequently, depletion of CHC, by perturbing the actin cytoskeleton and redistributing α-actinin, has a strong effect on the formation and maintenance of the contractile
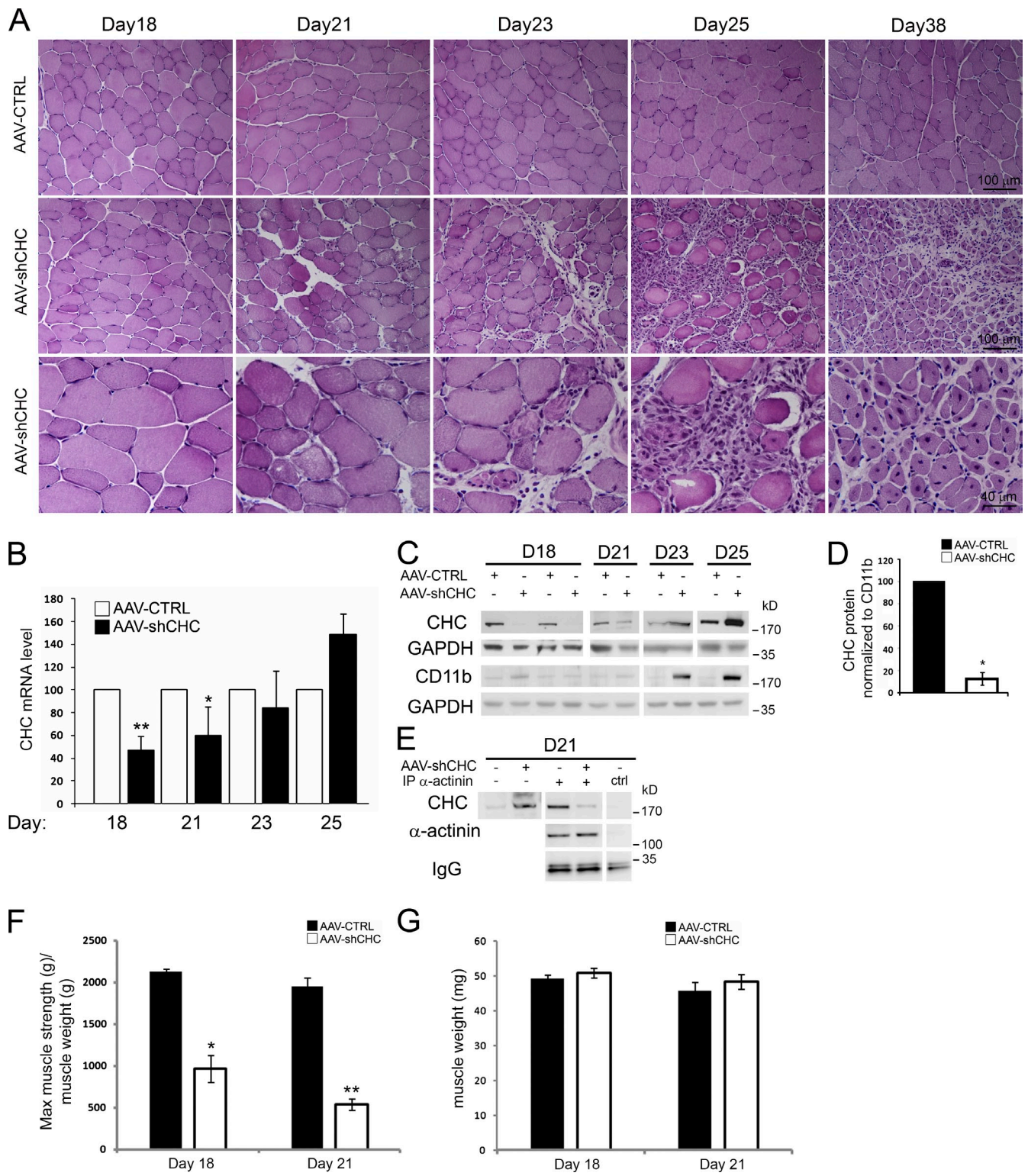
Figure 8. **CHC depletion using AAV-shCHC in vivo impairs force and causes muscle degeneration.** (A) Hematoxylin and eosin staining of AAV-CTRL– or AAV-shCHC–injected muscle at day 18, 21, 23, 25, and 38 after virus injection. (B) RT-qPCR of CHC mRNA levels at different time points after AAV-CTRL or shCHC AAV injection (n = 2–9 mice, data are presented as mean ± SD; *, $P < 0.05$; **, $P < 0.01$). (C) CHC protein levels at different time points after AAV-CTRL or shCHC AAV injection. The full time-course of CD11b levels, including the D23 and D25 time points shown here, is shown in Fig. S5 A. (D) Quantification of Western blot CHC band intensity (n = 4 mice at day 18, data are presented as mean ± SEM; *, $P < 0.05$; Mann-Whitney U test). (E) Immunoblot analysis of proteins associated with α-actinin or control immunoprecipitates of TA muscle lysates injected with AAV expressing a control construct or AAV expressing shCHC at 21 d after injection. (F and G) Measures of the specific maximal force (F) and of the muscle weight (G) of isolated TA muscle injected with AAV expressing a control construct or AAV expressing the shCHC construct (n = 3–5 mice) at either 18 or 21 d after injection. Data are presented as means ± SEM; for F: *, $P < 0.05$; **, $P < 0.01$.
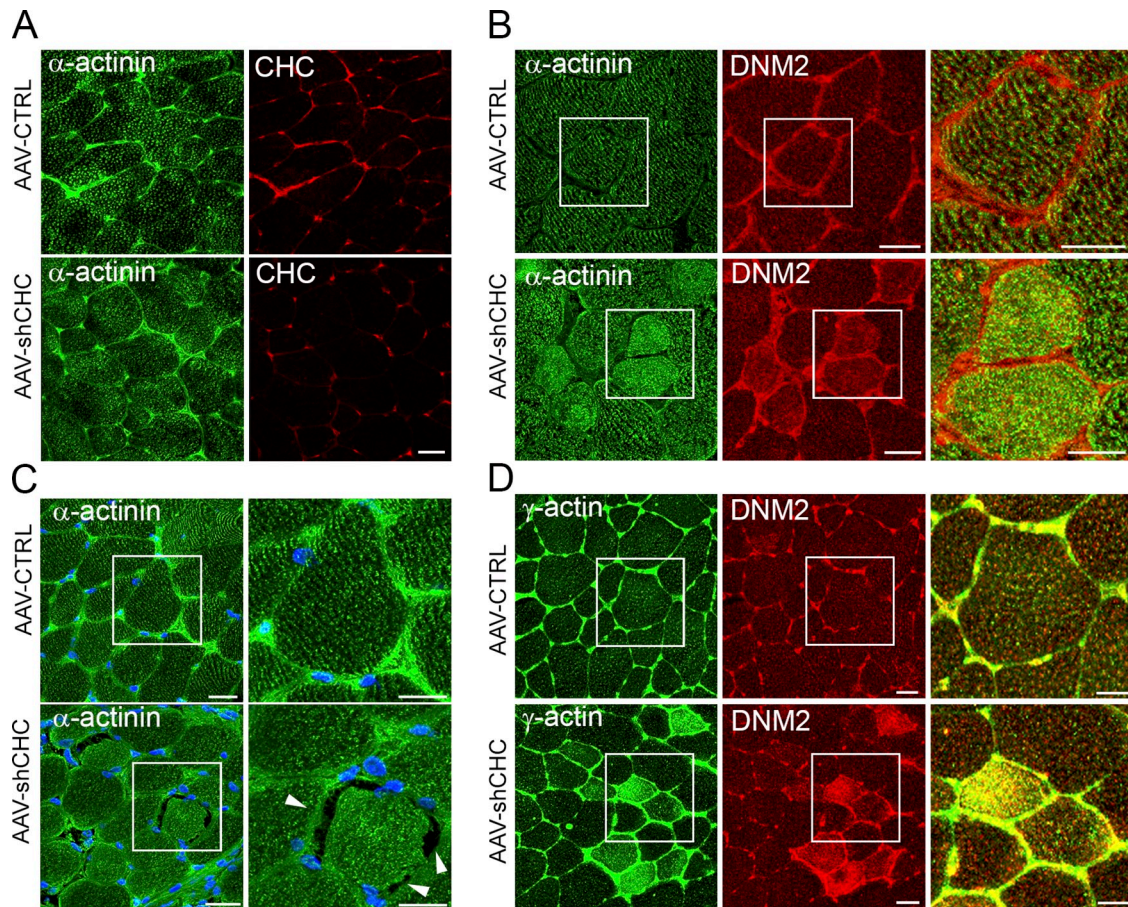
Figure 9.   **α-Actinin, γ-actin, and DNM2 distribution is perturbed upon in vivo CHC depletion.** (A–D) Confocal microscopy on transverse sections of skeletal muscle processed for double-immunofluorescent labeling using antibodies against (A) CHC (red) and α-actinin (green) at day 18 PI; (B) α-actinin (green) and DNM2 (red); (C) α-actinin (green) and DAPI (blue); (D) and γ-actin (green) and DNM2 (red) at day 21 PI. The boxed region in the merged images is magnified in the insets. Arrowheads point at regions of the fiber where the α-actinin staining is no longer associated with the sarcolemma. Bars: (main panels) 30 µm; (insets) 20 µm.

apparatus. The possibility that we are observing defective α-actinin trafficking inside the cell toward the PM is improbable because α-actinin is not a membrane-associated protein, does not colocalize with clathrin in intracellular compartments, and because AP1 and AP3 knockdown does not induce an α-actinin redistribution phenotype. In fact, our results clearly point toward a defect in the attachment of α-actinin to the cytoplasmic side of the PM and raise the possibility that clathrin is involved in actin scaffolding, thereby performing a task similar to what has been described for bacterial uptake, adherens junctions, and immune synapses (Bonazzi et al., 2011, 2012; Calabia-Linares et al., 2011). In addition, our results demonstrate a predominant role for AP2 in CHC targeting to the PM of differentiated myotubes.

The assembly of clathrin in plaques has been previously observed in several cell types, including muscle cells, but their physiological importance has proven controversial (De Deyne et al., 1998; Pumplin, 1989; Pumplin and Bloch, 1990; Akisaka et al., 2003; Bellve et al., 2006; Saffarian et al., 2009) and their functional role is still not clear. They were thought to represent artifacts of cell adhesion of cultured cells. However, large clathrin lattices have also been observed in non-adherent floating

cultured adipocytes (Bellve et al., 2006) and we observe them on non-adherent regions such as the top or the sides of myotubes (Fig. 2 D and Fig. S4 B). Because one putative role for clathrin-coated membrane domains is to maintain the stable attachment to the substrate, we suggest that clathrin plays the same role at the costamere, which is the muscle-specific adhesion site.

These large clathrin-coated plaques are also endocytically active, and invaginated pits are frequently observed at their edges. The implication of both CHC and DNM2 in focal adhesion turnover has previously been reported (Ezratty et al., 2005, 2009). Therefore, one may hypothesize that this protein complex responsible for formation and maintenance of the costameres is also involved in the turnover of these structures by endocytosis. In addition, we cannot exclude that the defects we are observing both in vitro and in vivo are at least partially due to defective endocytosis of costamere components. However, because (a) plaques in myotubes contain much more polymerized clathrin than would be required to form a single vesicle, (b) adhesion inhibits clathrin-mediated endocytosis (Batchelder and Yarar, 2010), and (c) endocytosis is reduced during differentiation (Kaisto et al., 1999), the defects we are observing
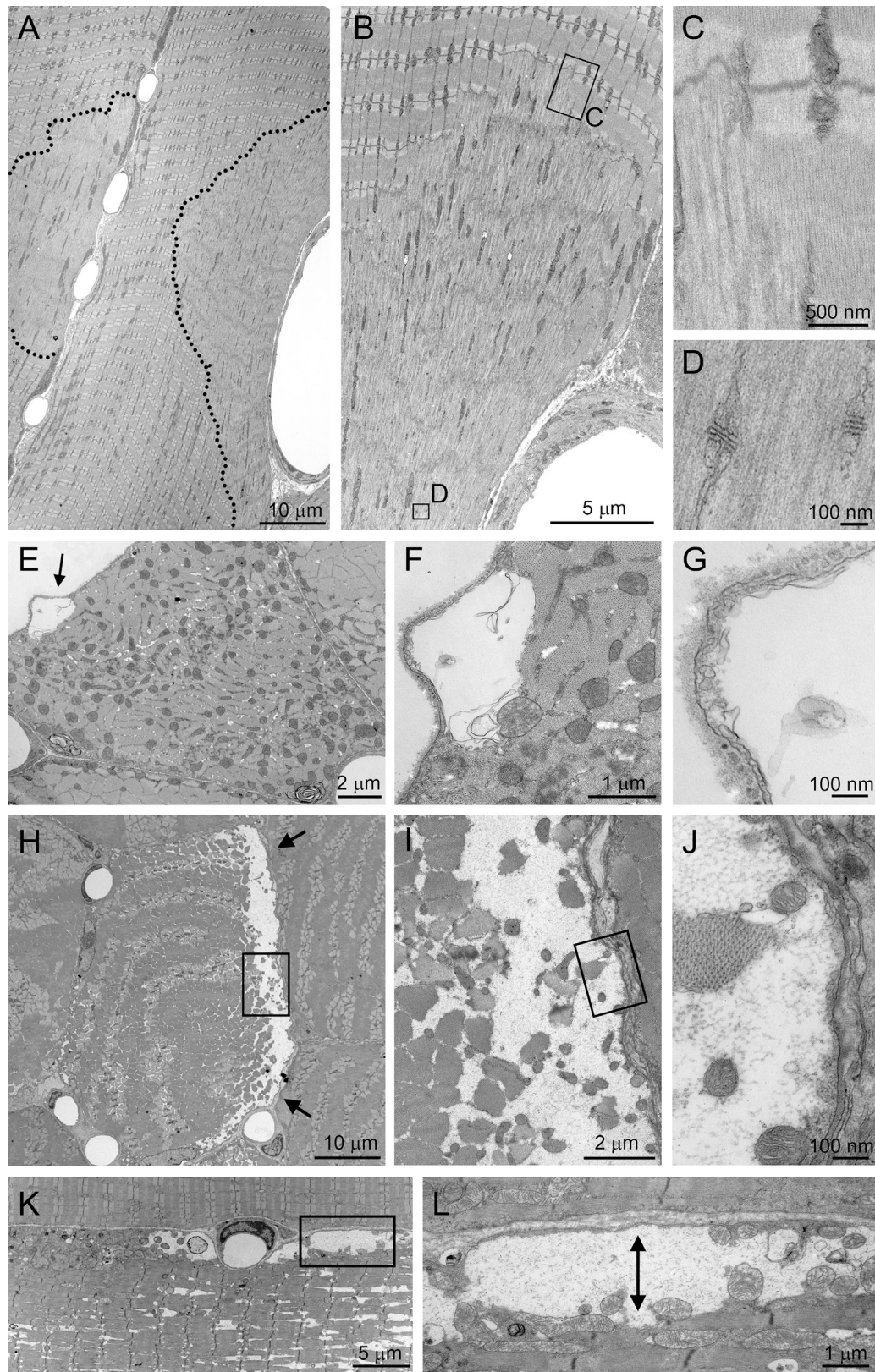
Figure 10. **Sarcomeric disorganization and detachment between sarcolemma and myofibrils upon in vivo CHC depletion.** Transmission electron microscopy of longitudinal (A–D, K–L) and transverse (E–J) muscle sections from mice injected with AAV-shCHC constructs at day 18 (A–G) and day 25 PI (H–L). In A–D, the sarcomeric apparatus is disorganized in focal regions adjoining the sarcolemma (within the dotted lines in A) and presents streaming and disassembly of the Z-line. C and D are insets of the respective boxed regions in B. In E–G, small detachments between the sarcolemma and the contractile apparatus are visible at day 18 PI. At day 25 PI, large detachments are seen in both transverse (H–J) and longitudinal orientation (K–L). I is an inset of the boxed region in H; J is an inset of the boxed region in I; L is an inset of the boxed region in K. Arrows in E, H, and L indicate detachments.

are probably not mainly due to endocytosis defects but could relate to the scaffolding role of CHC and DNM2 for the actin cytoskeleton (Schafer et al., 2002).

Our experiments show that these large clathrin-coated structures are intimately associated with the actin cytoskeleton and actin-binding proteins such as α-actinin. Because vinculin and talin were not detected in our coimmunoprecipitation experiments and because vinculin did not localize on clathrin-coated plaques (unpublished data), we believe that the coated domain corresponds to a different entity from classical focal adhesion contacts. The detection of clathrin plaques in situ in adult skeletal muscle is of great interest but remains technically challenging at the moment. It is of interest that costameres have been recurrently described as sub-sarcolemmal dense plaques (Chiesi et al., 1981; Pardo et al., 1983a,b; Shear and Bloch, 1985), and therefore it is tempting to speculate that part of the density which characterizes these structures could be attributed to clathrin plaques.

Early during in vivo clathrin depletion appear signs which point toward defects in costamere function. The first phenotype attributed to clathrin depletion is the presence of small detachments between the sarcolemma and the underlying myofibrils. CHC knockdown induces sarcomeric disorganization with streaming of the Z-line, which leads to a drastic and rapid muscle degeneration. Our in vivo experiments confirm the results obtained on differentiated myotubes and again point toward a role for CHC in the formation of stable plasma membrane compartments, which contributes to the attachment of sarcomeric lattices. Our results also point toward differences between three different costamere complexes. The first is centered on the DGC complex, dystrophin, ankyrins, and plectin (Ayalon et al., 2008; Randazzo et al., 2013), the second is centered on integrins, vinculin, α-actinin, and talin (Pardo et al., 1983a,b; Belkin et al., 1986), and the third is centered on integrins, α-actinin, and clathrin plaques (this paper); all three contain branched actin filaments. Also, the strong maximal force-loss seen in the clathrin-depleted muscle before any significant histological sign testifies to the vital role played by clathrin. The fact that more than 40% of the direct maximal force is lost before any change in total muscle mass or before the appearance of histological changes at the photon microscopy level could be attributed to the loss of both longitudinal and lateral force transmission in these myofibers. This force loss can be a direct consequence of both the large areas where disorganization of sarcomeres is evident and an uncoupling between the sarcolemma and the underlying contractile apparatus. Although the contribution of a trafficking dysfunction cannot be excluded, we believe that clathrin plays a structural role at the plasma membrane and that first appear signs related to this structural function.

Autosomal-dominant CNM is a rare neuromuscular disorder due to mutations in the *DNM2* gene (Bitoun et al., 2005). The results reported here and previous data suggest that impairment of CHC and DNM2 function in the formation and maintenance of the contractile apparatus via costamere organization may be relevant in CNM pathophysiology. Similarly to clathrin, DNM2 is mainly localized at the PM and the Z-line, where it colocalizes with α-actinin in both mouse and human skeletal

muscle (Cowling et al., 2011), and we show that DNM2 is required for proper α-actinin organization. Recently, a CNM-related *DNM2* mutation was associated with an accumulation of electron-dense material located between disorganized myofibrils as well as DNM2 and CHC mislocalization within the atrophied myofiber (Kierdaszuk et al., 2013). In addition, overexpression of DNM2 mutants in mouse skeletal muscle leads to α-actinin structural defects with prominent misalignment of the Z-line in vivo, which may explain at least in part the reduced specific maximal force observed in these mice (Cowling et al., 2011). All these data associated with the undeniable role of DNM2 in regulation of actin cytoskeleton dynamics and focal adhesion maintenance (Ezratty et al., 2005, 2009) highlight a new putative pathomechanism of *DNM2*-related CNM that merits further investigation.

Overall, our experiments clearly demonstrate the involvement of the CHC, the AP2 adaptor protein, Hip1R, and DNM2 in the formation of structures that, through association with α-actinin and actin filaments, allow the organization of the contractile apparatus in close association with the sarcolemma. The present study sheds light on a long-standing question, namely, the role of clathrin in skeletal muscle sarcomeric structure organization. Altogether, our results highlight an unconventional, novel role for clathrin in striated muscle that may be relevant to muscle physiology and whose dysfunction could be associated with the physiopathology of CNM linked to *DNM2* mutations.

Materials and methods

Antibodies
Anti-CHC mouse monoclonals X22 and TD.1, rabbit polyclonal against clathrin light chains (anti-consensus), and mouse monoclonal AP6 (against α-subunit of AP2) used in this study were produced by Dr. Brodsky's laboratory. The rabbit polyclonal antibody against CHC is from Abcam. For CHC detection in immunohistochemistry, immunocytochemistry, and electron microscopy we used the mouse monoclonal X22 antibody. The rabbit polyclonal was used for double-immunofluorescent labeling. Both X22 and the rabbit polyclonal anti-CHC completely colocalize. For Western blot experiments, both mouse monoclonal TD.1 and rabbit polyclonal (Abcam) antibodies were used. Other commercial sources of antibodies were as follows: mouse monoclonals against α-actinin 2, smooth-muscle actin, γ-actin, vinculin, and talin (Sigma-Aldrich); mouse monoclonal SA4 against AP3 (δ-subunit DSHB); rabbit polyclonal against AP1 (γ-subunit); rabbit polyclonal anti-DNM2, rabbit polyclonal anti-integrin β5, rabbit polyclonal anti-GAPDH, and rabbit polyclonal anti-CD11b (Abcam); goat polyclonal anti-caveolin3 (Santa Cruz Biotechnology, Inc.); rabbit polyclonal against dystrophin and mouse monoclonal against β-dystroglycan (Novocastra); and rabbit polyclonal against Hip1R (EMD Millipore). Secondary antibodies for immunofluorescence were from Life Technologies (Alexa Fluor 488, 568, and 633 conjugates). Secondary antibodies coupled to horseradish peroxidase were from Jackson ImmunoResearch Laboratories, Inc.

Muscle tissue lysate
Lysates of whole tissue were prepared from freshly dissected mouse skeletal muscle. Tissue was homogenized by dounce in lysis buffer (1 mg/3 ml 50 mM Tris-HCl, pH 7.5, 0.15 M NaCl, 1 mM EDTA, 1% NP-40, and 1 protease inhibitor cocktail tablet [1:10 ml buffer; Roche]). Homogenate was centrifuged for 10 min at 14,000 g, and the pellet discarded to obtain a post-nuclear supernatant. Protein concentration of the lysate was determined by Bradford assay (Bio-Rad Laboratories).

Immunoblot analysis
Protein samples were separated by electrophoresis (4–12% bis-acrylamide gel; Life Technologies), then electrophoretically transferred to 0.45-µm nitrocellulose membranes (Life Technologies) and labeled with primary antibodies and secondary antibodies coupled to horseradish peroxidase.

The presence of proteins in samples was detected using Western Lightning chemiluminescence reagent (GE Healthcare). Quantification was performed using Quantity One software (Bio-Rad Laboratories).

Subcellular fractionation

3T3 fibroblasts, C2C12 myoblasts, and differentiated C2C12 myotubes were homogenized in HES buffer at pH 7.4 (20 mM Hepes, 1 mM EDTA, and 225 mM sucrose) by passing 10× through a 27-gauge needle. Homogenates were centrifuged for 20 min at 19,000 g. The resulting pellets were resuspended in HES buffer, layered on top of a 1.12-M sucrose cushion and centrifuged at 101,000 g for 60 min at 4°C. The PM fraction was collected from the interface of the two solutions. Centrifugation of the initial supernatant (212,000 g) for 60 min at 4°C allowed separation of the intracellular membrane fraction (pellet) and cytosol (supernatant).

Immunoprecipitation

For 3T3 and C2C12 subcellular fractions (PM and cytosol), 250 µl of each fraction was diluted to half using lysis buffer (50 mM Tris-HCl, pH 7.5, 0.15 M NaCl, 1 mM EDTA, 1% NP-40, and 1 protease inhibitor cocktail tablet [1:10 ml buffer; Roche]). Mouse skeletal muscle tissue lysate (postnuclear supernatant) was diluted to 3 mg/ml in lysis buffer, precleared with 30 µl washed protein G–Sepharose (PGS 4 fast flow; GE Healthcare) per 400 µl of diluted lysate, and incubated with 20 µg of specific antibody overnight (4°C). Then 30 µl washed PGS was added and incubated for 1 h at 4°C. Pelleted PGS was taken up in sample buffer and subjected to electrophoresis and immunoblotting. For all immunoprecipitation experiments, HRP-conjugated rabbit and mouse IgG TrueBlot secondary antibodies (eBioscience) were used.

Dissociated fiber cultures

Myofibers were isolated from the dissected FDB muscle of 6-wk-old mice by digestion with collagenase 1a (Worthington Biochemical Corporation) and mechanical dissociation. Isolated fibers were cultured (37°C, 5% CO$_2$) in DMEM with high glucose, 1% horse serum (Gibco), and penicillin/streptomycin on coverslips coated with Matrigel (BD). Myofibers were transduced with 70 µl of AAV vector (7×10^{10} viral genomes/well) for 12 d.

Mouse myoblast cultures

Primary skeletal muscle cells and C2C12 cells were maintained in tissue culture dishes coated with rat tail collagen in basal medium with 20% fetal bovine serum (FBS), 50 U/ml penicillin, and 50 mg/ml streptomycin (growth medium). Differentiation was induced when cells were ∼80% confluent by culturing in differentiation medium (basal medium with 2% horse serum). For siRNA treatment, cells (differentiated for either 4 or 6 d) were transfected using 10 nM siRNA and transfection reagent (jetPRIME; Poly-Plus Transfection) according to the manufacturer's instructions. Targeting and GAPDH-specific control siRNAs were synthesized by Eurogentec. For CHC, sequences targeted were similar to those used in Ezratty et al. (2009): 5′-AACAUUGGCUUCAGUACCUUG-3′ for CHC-1, 5′-AAUGGAUCU-CUUUGAAUACGG-3′ for CHC-2, and 5′-GAGCAUGUGCACGCUGGC-CAGCU-3′ for the α-subunit of AP2. The GAPDH siRNA sequence was 5′-AAAGUUGUCAUGGAUGACC-3′ and was used as a negative control in all siRNA experiments. The sequence of the siRNA specific for the γ-subunit of the AP1 complex (γ-adaptin) was 5′-AGCUAUGAAUGAUAUAUUA-3′, which is similar to the sequence used in Dugast et al. (2005) and Braun et al. (2007). The sequence of the siRNA specific for the δ-subunit of the AP3 complex (δ-adaptin) was 5′-CAUCAAGAUCAUCAAGCUG-3′, which is similar to the sequence used in Braun et al. (2007). The sequence of the siRNA specific for DNM2 was 5′-ACCUACAUCAGGGAGCGAGAA-3′. The sequence of the siRNA specific for Hip1R was 5′-AACUCCUGCA-CAGACCUGAUG-3′, which is similar to the sequence used in Engqvist-Goldstein et al. (2004). For CHC depletion, cells were transfected twice for 48 h. For all other siRNA constructs, cells were transfected once for 48–72 h.

Immunofluorescence microscopy

Adult mouse skeletal muscle was embedded in Tissue-Tek OCT compound (Miles, Inc.), frozen, and stored at −80°C. Cryosections (10-µm thick) were fixed (15 min, 4% paraformaldehyde in PBS or 10 min, 95% ethanol [Fig. 1 D] at room temperature [RT]), permeabilized (5 min, 0.5% Triton X-100 in PBS at RT), and blocked (30 min, PBS with 0.1% Triton X-100, 5% bovine serum albumin [BSA]). Sections were incubated with primary antibodies (overnight, 4°C, in PBS with 0.1% Triton X-100 and 5% BSA) and washed in PBS with 0.1% Triton X-100. Sections were then incubated with secondary antibodies (60 min at RT), washed in PBS with 0.1% Triton X-100, and mounted with anti-fading solution (DABCO) containing 300 nM DAPI. For double labeling, the two primary antibodies (from different

species) or the two secondary antibodies were added simultaneously at the appropriate step. Secondary antibodies were labeled with either Alexa Fluor 488 or Alexa Fluor 568.

For myofibers isolated from mouse muscle, immunolabeling was performed directly in the 24-well culture plate. Cells were fixed (15 min, 4% paraformaldehyde in PBS at RT), permeabilized (10 min in PBS with 0.5% Triton X-100), and immunolabeled using the same procedure described for mouse muscle sections.

For mouse cells grown on coverslips, cells were washed in warm PBS, fixed in paraformaldehyde (4% in PBS, 15 min), then washed in PBS, permeabilized (10 min, 0.5% Triton X-100 in PBS) and blocked in blocking solution (5% BSA in PBS with 0.1% Triton X-100, 30 min). Antibody labeling was performed by addition of 200 µl blocking solution with primary or secondary antibodies (1–5 µg/ml) and washing with PBS with 0.1% Triton X-100. Samples were mounted in Vectashield containing DAPI (Vector Laboratories).

Muscle sections, mouse cells, and myofibers from mouse muscle were analyzed by confocal laser scanning microscopy using an inverted operating system (SP2; Leica) equipped with HCX Plan-Apo CS 40×/1.20 NA and 63×/1.40 NA oil immersion objective lenses. Images presented in Figs. 1 A, 5, 6, S3, and S4 were acquired using an upright confocal laser scanning microscope (FV-1000; Olympus) equipped with a UPlanS-Apo 60×/1.35 NA oil immersion objective lens. DAPI, Alexa Fluor 488, and Alexa Fluor 568 fluorescence was sequentially excited using lasers with wavelengths of 405 for DAPI, 488 (Leica) or 473 (Olympus) for Alexa Fluor 488, and 543 nm for Alexa Fluor 568. Z-series from the top to the bottom of fibers were sequentially collected for each channel with a step of 0.9–1 µm between each frame. Imaging was performed at room temperature using Type F immersion oil (Leica). Images (1024 × 1024 pixels) were saved as TIFF files in Olympus FV-1000 software and Leica confocal software, and input levels were adjusted in Adobe Photoshop. Image quantification was performed using ImageJ (National Institutes of Health).

Image analysis

Striated surface measurement. The α-actinin striated surface per myotube was quantified by manually drawing a region of interest in ImageJ around the striated or total cell surface in a single Z-stack from the middle of the cell. The striated surface was obtained by performing the ratio between striated and total myotube surface.

α-Actinin aggregate size analysis. The "Analyze Particles" ImageJ plugin (version 1.46) was used to count intracellular particles on binary confocal images of C2C12 myotubes in a single Z-stack from the middle of the cell and to automatically measure the number and area of these particles.

shRNA constructs

The siRNA against CHC (CHC-1) used for in vitro transfection experiments was synthesized to be directly cloned in pSUPER under the control of the H1 promoter. ShRNA consisted of a 21-nt sense sequence followed by a 9-nt loop (TTCAAGAGA), a 19-nt reverse sequence, and an RNA pol III terminator (TTTTT). The H1 cassette was then introduced into an AAV1-based vector between the two ITRs using the blunted SpeI and SalI sites on pSUPER-shRNA plasmid and the XbaI site on the pSMD2 AAV2 vector backbones, which were type 1 pseudotyped (Généthon).

Virus production and titration

AAV2/1 pseudotyped vectors were prepared by transfection in 293 cells as described previously (Rivière et al., 2006) using the pSMD2-shRNA plasmid, the pXX6 plasmid (Généthon) coding for the adenoviral sequences essential for AAV production, and the pRepCAp plasmid (Généthon) coding for AAV1 capsid. Vector particles were purified on iodixanol gradients and concentrated on Amicon Ultra-15 100K columns (EMD Millipore). The final viral preparations were kept in PBS solution at −80°C. The particle titer (number of viral genomes) was determined by quantitative PCR. Titers for AAV shCHC were 4×10^{12} vector genomes (vg)/ml.

In vivo gene transfer

Experiments were performed on adult 8-wk-old C57/BL6 mice. Anesthesia was achieved with a mix of 100 mg/kg ketamine and 10 mg/kg xylasine or using isoflurane. Two intramuscular injections (40 µl/TA), 24 h apart of AAV-shCHC, was performed in TA of the right hindlimb; the contralateral muscles were injected using the same procedure with control AAV vector (AAV-CTRL), which expresses the muSEAP protein (murine-secreted embryonic alkaline phosphatase). Mice were sacrificed at different intervals after the injection.

Gene expression analysis

Total RNA was prepared from 400-µm cryostat sections of TA using the Nucleospin RNAII kit (Macherey-Nagel). Complementary DNA generated with the Superscript II Plus reverse transcription kit (Life Technologies) was analyzed by real-time qPCR performed on an Opticon2 system (Bio-Rad Laboratories) using iTaq SyberGreen Supermix with ROX (Bio-Rad Laboratories). In all samples, we quantified transcript of the *PO* gene encoding mouse acidic ribosomal phosphoprotein ubiquitously expressed as endogenous RNA control, and each sample was normalized on the basis of its PO content. Primers used for CHC: forward exon 6, 5′-GAGTCAAC-AGAAAGGGACA-3′; reverse exon 7, 5′-CATTCTCAGAGCCAAGTCAG-3′. Primers used for PO: forward, 5′-CTCCAAGCAGATGCAGCAGA-3′; reverse, 5′-ATAGCCTTGCGCATCATGGT-3′.

Histomorphological and ultrastructural analyses

Samples were frozen in liquid nitrogen–cooled isopentane. Transverse sections of TA muscle (8-µm thick) were stained with H&E by standard methods. Light microscopy was performed using an upright microscope (DMR; Leica) and a 40×/NA 0.85 HCX Plan Apo objective (Leica). Images were captured using a monochrome camera (DS-Ri1; Nikon) and NIS-Elements BR software (Nikon). For all imaging, exposure settings were identical between compared samples and viewed at room temperature.

For morphological electron microscopy, muscles were fixed by intra-aortic perfusion with 2% paraformaldehyde and 2% glutaraldehyde in 0.1 M phosphate buffer (pH 7.4). TA samples were post-fixed with 2% OsO_4, in 0.1 M phosphate buffer (pH 7.4) for 1 h, then dehydrated in a graded series of acetone including a 1% uranyl acetate staining step in 70% acetone and finally embedded in epon resin. For pre-embedding immunogold clathrin labeling, mice were fixed with 2% paraformaldehyde and TA longitudinal 100-µm-thick sections were cut with a vibratome. Then a standard free-floating immunocytochemical procedure was followed, using 0.1 M saline phosphate buffer as diluent and rinsing liquids. After pre-incubation in 5% normal goat serum, 5% BSA, sections were incubated overnight at 4°C in 1:500 anti-clathrin antibody. A further 4-h incubation in ultra-small gold conjugate of goat anti–rabbit IgG (1:20; Aurion) was followed by extensive washings, 10 min post-fixation in 2% glutaraldehyde, and 0.70-nm gold beads were then silver enhanced (HQ silver; Nanoprobes). After 15 min post-fixation in 1% OsO_4, sections were dehydrated in graded acetone and embedded in epon resin.

Thin (70 nm) sections were stained with uranyl acetate and lead citrate, and in some cases (Fig. 1 F) a 1% tannic acid (1 min) staining step preceded uranyl staining. Observations were made on an electron microscope (model CM120; Philips) and images were recorded with a Morada digital camera (Olympus).

Electron microscopy of unroofed myotubes

Adherent PM from myotubes cultured as described above were prepared for rapid-freeze, deep-etch electron microscopy as described previously (Heuser, 2000). In brief, cells grown on small oriented pieces of glass coverslip were disrupted by sonication, fixed in paraformaldehyde, and labeled with anti-clathrin (X22), anti–α-actinin, or anti–β5 integrin and then 18-nm gold-conjugated anti–mouse or anti–rabbit antibody. Each water-washed coverslip is mounted on a 3 × 3-mm slab of aldehyde-fixed and water-washed rabbit lung (0.8-mm thick) that serves as a cushion for the next step. Then it is quick-frozen by abrupt impact against an ultrapure copper block cooled to 4 degrees above absolute zero. The coverslip is stored in liquid nitrogen until mounting in a vacuum evaporator (model 301; Balzers). In this device, it is next freeze-dried by warming it to −80°C for 15 min, and is then rotary-replicated with a thin (∼2 nm) film of platinum evaporated over 5–10 s from an electron beam gun mounted 15–20 degrees above the horizontal, all while the coverslip is rotated at 5 Hz. This "replica" of the coverslip and the cells remaining attached to it is supported by evaporating ∼10 nm of pure carbon onto it, using a standard carbon-arc supply mounted 10 degrees off the vertical. The resultant platinum replica is floated off the glass by angled immersion into full-strength (47%) hydrofluoric acid, washed several times by floatation on distilled water, and picked up on 75 mesh formvar-coated EM grids. The grid is mounted in a eucentric side-entry goniometer stage of a transmission electron microscope (model 1400; JEOL USA, Inc.) equipped with a high-resolution 4K AMT digital camera. Images were processed in Adobe Photoshop to adjust brightness and contrast.

Contractile properties

The isometric contractile properties of TA muscles were studied in situ on mice anesthetized with 60 mg/kg pentobarbital. The distal tendon of the TA muscle was attached to a lever arm of a servomotor system (305B Dual-Mode Lever; Aurora Scientific). Muscles were directly stimulated by a bipolar silver electrode using a supramaximal (80 V) square wave pulse of 0.1-ms duration. Absolute maximal force (P_0) was measured during isometric contractions in response to electrical stimulation (frequency of 25–150 Hz; train of stimulation of 500 ms). All isometric contraction measurements were made at optimal muscle length (L_0) at which P_0 was obtained. TA muscles were weighted and specific maximal force (sP_0) was calculated by dividing P_0 by muscle weight.

Statistics and institutional guideline compliance

Statistical analysis was performed using Student's *t* test except as otherwise stated. All animal studies were performed in compliance with the French government guidelines.

Online supplemental material

Fig. S1 shows ultrastructural analysis of tannic acid–stained muscle sections, anti-CHC–labeled muscle sections, and ultrastructural localization of clathrin in clathrin-coated pits and plaques of unroofed mouse primary myotubes. Fig. S2 displays additional images of α-actinin localization and localization of β5-integrin in clathrin plaques of mouse primary myotubes. Fig. S3 shows efficiency of siRNA-mediated AP1, AP2, AP3, DNM2, and Hip1R depletion, the effect of siRNA-mediated AP2 depletion on CHC distribution, and localization of Hip1R in control and CHC- or AP2-depleted myotubes. Fig. S4 compares the effect of siRNA-mediated depletion of CHC, AP1, AP2, Hip1R, and DNM2 on actin distribution, and characterizes localization of DNM2 in control or CHC- and AP2-depleted myotubes. Fig. S5 shows that in vivo CHC depletion induces a strong inflammatory response but has no effect of β-dystroglycan and dystrophin distribution. Online supplemental material is available at http://www.jcb.org/cgi/content/full/jcb.201309096/DC1. Additional data are available in the JCB DataViewer at http://dx.doi.org/10.1083/jcb.201309096.dv.

References

Akisaka, T., H. Yoshida, R. Suzuki, K. Shimizu, and K. Takama. 2003. Clathrin sheets on the protoplasmic surface of ventral membranes of osteoclasts in culture. *J. Electron Microsc. (Tokyo).* 52:535–543. http://dx.doi.org/10.1093/jmicro/52.6.535

Ayalon, G., J.Q. Davis, P.B. Scotland, and V. Bennett. 2008. An ankyrin-based mechanism for functional organization of dystrophin and dystroglycan. *Cell.* 135:1189–1200. http://dx.doi.org/10.1016/j.cell.2008.10.018

Batchelder, E.M., and D. Yarar. 2010. Differential requirements for clathrin-dependent endocytosis at sites of cell-substrate adhesion. *Mol. Biol. Cell.* 21:3070–3079. http://dx.doi.org/10.1091/mbc.E09-12-1044

Belkin, A.M., N.I. Zhidkova, and V.E. Koteliansky. 1986. Localization of talin in skeletal and cardiac muscles. *FEBS Lett.* 200:32–36. http://dx.doi.org/10.1016/0014-5793(86)80505-1

Bellve, K.D., D. Leonard, C. Standley, L.M. Lifshitz, R.A. Tuft, A. Hayakawa, S. Corvera, and K.E. Fogarty. 2006. Plasma membrane domains specialized for clathrin-mediated endocytosis in primary cells. *J. Biol. Chem.* 281:16139–16146. http://dx.doi.org/10.1074/jbc.M511370200

Bitoun, M., S. Maugenre, P.Y. Jeannet, E. Lacène, X. Ferrer, P. Laforêt, J.J. Martin, J. Laporte, H. Lochmüller, A.H. Beggs, et al. 2005. Mutations in dynamin 2 cause dominant centronuclear myopathy. *Nat. Genet.* 37:1207–1209. http://dx.doi.org/10.1038/ng1657

Blake, D.J., A. Weir, S.E. Newey, and K.E. Davies. 2002. Function and genetics of dystrophin and dystrophin-related proteins in muscle. *Physiol. Rev.* 82:291–329.

Bonazzi, M., L. Vasudevan, A. Mallet, M. Sachse, A. Sartori, M.C. Prevost, A. Roberts, S.B. Taner, J.D. Wilbur, F.M. Brodsky, and P. Cossart. 2011. Clathrin phosphorylation is required for actin recruitment at sites of bacterial adhesion and internalization. *J. Cell Biol.* 195:525–536. http://dx.doi.org/10.1083/jcb.201105152

Bonazzi, M., A. Kühbacher, A. Toledo-Arana, A. Mallet, L. Vasudevan, J. Pizarro-Cerdá, F.M. Brodsky, and P. Cossart. 2012. A common clathrin-mediated machinery co-ordinates cell-cell adhesion and bacterial internalization. *Traffic.* 13:1653–1666. http://dx.doi.org/10.1111/tra.12009

Braun, V., C. Deschamps, G. Raposo, P. Benaroch, A. Benmerah, P. Chavrier, and F. Niedergang. 2007. AP-1 and ARF1 control endosomal dynamics at sites of FcR mediated phagocytosis. *Mol. Biol. Cell.* 18:4921–4931. http://dx.doi.org/10.1091/mbc.E07-04-0392

Brodsky, F.M. 1985. Clathrin structure characterized with monoclonal antibodies. II. Identification of in vivo forms of clathrin. *J. Cell Biol.* 101:2055–2062. http://dx.doi.org/10.1083/jcb.101.6.2055

Brodsky, F.M. 2012. Diversity of clathrin function: new tricks for an old protein. *Annu. Rev. Cell Dev. Biol.* 28:309–336. http://dx.doi.org/10.1146/annurev-cellbio-101011-155716

Burridge, K., J. Feramisco, and S. Blose. 1980. The association of alpha-actinin and clathrin with the plasma membrane. *Prog. Clin. Biol. Res.* 41:907–924.

Butler, M.H., C. David, G.C. Ochoa, Z. Freyberg, L. Daniell, D. Grabs, O. Cremona, and P. De Camilli. 1997. Amphiphysin II (SH3P9; BIN1), a member of the amphiphysin/Rvs family, is concentrated in the cortical cytomatrix of axon initial segments and nodes of ranvier in brain and around T tubules in skeletal muscle. *J. Cell Biol.* 137:1355–1367. http://dx.doi.org/10.1083/jcb.137.6.1355

Calabia-Linares, C., J. Robles-Valero, H. de la Fuente, M. Perez-Martinez, N. Martín-Cofreces, M. Alfonso-Pérez, C. Gutierrez-Vázquez, M. Mittelbrunn, S. Ibiza, F.R. Urbano-Olmos, et al. 2011. Endosomal clathrin drives actin accumulation at the immunological synapse. *J. Cell Sci.* 124:820–830. http://dx.doi.org/10.1242/jcs.078832

Chen, C.Y., and F.M. Brodsky. 2005. Huntingtin-interacting protein 1 (Hip1) and Hip1-related protein (Hip1R) bind the conserved sequence of clathrin light chains and thereby influence clathrin assembly in vitro and actin distribution in vivo. *J. Biol. Chem.* 280:6109–6117. http://dx.doi.org/10.1074/jbc.M408454200

Chiesi, M., M.M. Ho, G. Inesi, A.V. Somlyo, and A.P. Somlyo. 1981. Primary role of sarcoplasmic reticulum in phasic contractile activation of cardiac myocytes with shunted myolemma. *J. Cell Biol.* 91:728–742. http://dx.doi.org/10.1083/jcb.91.3.728

Collins, A., A. Warrington, K.A. Taylor, and T. Svitkina. 2011. Structural organization of the actin cytoskeleton at sites of clathrin-mediated endocytosis. *Curr. Biol.* 21:1167–1175. http://dx.doi.org/10.1016/j.cub.2011.05.048

Cowling, B.S., A. Toussaint, L. Amoasii, P. Koebel, A. Ferry, L. Davignon, I. Nishino, J.L. Mandel, and J. Laporte. 2011. Increased expression of wild-type or a centronuclear myopathy mutant of dynamin 2 in skeletal muscle of adult mice leads to structural defects and muscle weakness. *Am. J. Pathol.* 178:2224–2235. http://dx.doi.org/10.1016/j.ajpath.2011.01.054

De Deyne, P.G., A. O'Neill, W.G. Resneck, G.M. Dmytrenko, D.W. Pumplin, and R.J. Bloch. 1998. The vitronectin receptor associates with clathrin-coated membrane domains via the cytoplasmic domain of its beta5 subunit. *J. Cell Sci.* 111:2729–2740.

Dlugosz, A.A., P.B. Antin, V.T. Nachmias, and H. Holtzer. 1984. The relationship between stress fiber-like structures and nascent myofibrils in cultured cardiac myocytes. *J. Cell Biol.* 99:2268–2278. http://dx.doi.org/10.1083/jcb.99.6.2268

Dugast, M., H. Toussaint, C. Dousset, and P. Benaroch. 2005. AP2 clathrin adaptor complex, but not AP1, controls the access of the major histocompatibility complex (MHC) class II to endosomes. *J. Biol. Chem.* 280:19656–19664. http://dx.doi.org/10.1074/jbc.M501357200

Durieux, A.C., A. Vignaud, B. Prudhon, M.T. Viou, M. Beuvin, S. Vassilopoulos, B. Fraysse, A. Ferry, J. Lainé, N.B. Romero, et al. 2010. A centronuclear myopathy-dynamin 2 mutation impairs skeletal muscle structure and function in mice. *Hum. Mol. Genet.* 19:4820–4836. http://dx.doi.org/10.1093/hmg/ddq413

Engqvist-Goldstein, A.E., R.A. Warren, M.M. Kessels, J.H. Keen, J. Heuser, and D.G. Drubin. 2001. The actin-binding protein Hip1R associates with clathrin during early stages of endocytosis and promotes clathrin assembly in vitro. *J. Cell Biol.* 154:1209–1223. http://dx.doi.org/10.1083/jcb.200106089

Engqvist-Goldstein, A.E., C.X. Zhang, S. Carreno, C. Barroso, J.E. Heuser, and D.G. Drubin. 2004. RNAi-mediated Hip1R silencing results in stable association between the endocytic machinery and the actin assembly machinery. *Mol. Biol. Cell.* 15:1666–1679. http://dx.doi.org/10.1091/mbc.E03-09-0639

Epstein, H.F., and D.A. Fischman. 1991. Molecular analysis of protein assembly in muscle development. *Science.* 251:1039–1044. http://dx.doi.org/10.1126/science.1998120

Ervasti, J.M. 2003. Costameres: the Achilles' heel of Herculean muscle. *J. Biol. Chem.* 278:13591–13594. http://dx.doi.org/10.1074/jbc.R200021200

Esk, C., C.Y. Chen, L. Johannes, and F.M. Brodsky. 2010. The clathrin heavy chain isoform CHC22 functions in a novel endosomal sorting step. *J. Cell Biol.* 188:131–144. http://dx.doi.org/10.1083/jcb.200908057

Ezratty, E.J., M.A. Partridge, and G.G. Gundersen. 2005. Microtubule-induced focal adhesion disassembly is mediated by dynamin and focal adhesion kinase. *Nat. Cell Biol.* 7:581–590. http://dx.doi.org/10.1038/ncb1262

Ezratty, E.J., C. Bertaux, E.E. Marcantonio, and G.G. Gundersen. 2009. Clathrin mediates integrin endocytosis for focal adhesion disassembly in migrating cells. *J. Cell Biol.* 187:733–747. http://dx.doi.org/10.1083/jcb.200904054

Fausser, J.L., E. Ungewickell, J.V. Ruch, and H. Lesot. 1993. Interaction of vinculin with the clathrin heavy chain. *J. Biochem.* 114:498–503.

Fujimoto, L.M., R. Roth, J.E. Heuser, and S.L. Schmid. 2000. Actin assembly plays a variable, but not obligatory role in receptor-mediated endocytosis in mammalian cells. *Traffic.* 1:161–171. http://dx.doi.org/10.1034/j.1600-0854.2000.010208.x

Heuser, J. 1980. Three-dimensional visualization of coated vesicle formation in fibroblasts. *J. Cell Biol.* 84:560–583. http://dx.doi.org/10.1083/jcb.84.3.560

Heuser, J. 2000. The production of 'cell cortices' for light and electron microscopy. *Traffic.* 1:545–552. http://dx.doi.org/10.1034/j.1600-0854.2000.010704.x

Kaisto, T., P. Rahkila, V. Marjomäki, R.G. Parton, and K. Metsikkö. 1999. Endocytosis in skeletal muscle fibers. *Exp. Cell Res.* 253:551–560. http://dx.doi.org/10.1006/excr.1999.4659

Kaufman, S.J., D. Bielser, and R.F. Foster. 1990. Localization of anti-clathrin antibody in the sarcomere and sensitivity of myofibril structure to chloroquine suggest a role for clathrin in myofibril assembly. *Exp. Cell Res.* 191:227–238. http://dx.doi.org/10.1016/0014-4827(90)90009-Y

Kierdaszuk, B., M. Berdynski, J. Karolczak, M.J. Redowicz, C. Zekanowski, and A.M. Kaminska. 2013. A novel mutation in the DNM2 gene impairs dynamin 2 localization in skeletal muscle of a patient with late onset centronuclear myopathy. *Neuromuscul. Disord.* 23:219–228. http://dx.doi.org/10.1016/j.nmd.2012.12.007

Kirchhausen, T. 1999. Adaptors for clathrin-mediated traffic. *Annu. Rev. Cell Dev. Biol.* 15:705–732. http://dx.doi.org/10.1146/annurev.cellbio.15.1.705

Legendre-Guillemin, V., M. Metzler, J.F. Lemaire, J. Philie, L. Gan, M.R. Hayden, and P.S. McPherson. 2005. Huntingtin interacting protein 1 (HIP1) regulates clathrin assembly through direct binding to the regulatory region of the clathrin light chain. *J. Biol. Chem.* 280:6101–6108. http://dx.doi.org/10.1074/jbc.M408430200

Merisko, E.M. 1985. Evidence for the interaction of alpha-actinin and calmodulin with the clathrin heavy chain. *Eur. J. Cell Biol.* 39:167–172.

Merisko, E.M., J.K. Welch, T.Y. Chen, and M. Chen. 1988. Alpha-actinin and calmodulin interact with distinct sites on the arms of the clathrin trimer. *J. Biol. Chem.* 263:15705–15712.

Merrifield, C.J., M.E. Feldman, L. Wan, and W. Almers. 2002. Imaging actin and dynamin recruitment during invagination of single clathrin-coated pits. *Nat. Cell Biol.* 4:691–698. http://dx.doi.org/10.1038/ncb837

Pardo, J.V., J.D. Siliciano, and S.W. Craig. 1983a. A vinculin-containing cortical lattice in skeletal muscle: transverse lattice elements ("costameres") mark sites of attachment between myofibrils and sarcolemma. *Proc. Natl. Acad. Sci. USA.* 80:1008–1012. http://dx.doi.org/10.1073/pnas.80.4.1008

Pardo, J.V., J.D. Siliciano, and S.W. Craig. 1983b. Vinculin is a component of an extensive network of myofibril-sarcolemma attachment regions in cardiac muscle fibers. *J. Cell Biol.* 97:1081–1088. http://dx.doi.org/10.1083/jcb.97.4.1081

Pearse, B.M., and M.S. Robinson. 1990. Clathrin, adaptors, and sorting. *Annu. Rev. Cell Biol.* 6:151–171. http://dx.doi.org/10.1146/annurev.cb.06.110190.001055

Pumplin, D.W. 1989. Acetylcholine receptor clusters of rat myotubes have at least three domains with distinctive cytoskeletal and membranous components. *J. Cell Biol.* 109:739–753. http://dx.doi.org/10.1083/jcb.109.2.739

Pumplin, D.W., and R.J. Bloch. 1990. Clathrin-coated membrane: a distinct membrane domain in acetylcholine receptor clusters of rat myotubes. *Cell Motil. Cytoskeleton.* 15:121–134. http://dx.doi.org/10.1002/cm.970150208

Quach, N.L., and T.A. Rando. 2006. Focal adhesion kinase is essential for costamerogenesis in cultured skeletal muscle cells. *Dev. Biol.* 293:38–52. http://dx.doi.org/10.1016/j.ydbio.2005.12.040

Randazzo, D., E. Giacomello, S. Lorenzini, D. Rossi, E. Pierantozzi, B. Blaauw, C. Reggiani, S. Lange, A.K. Peter, J. Chen, and V. Sorrentino. 2013. Obscurin is required for ankyrinB-dependent dystrophin localization and sarcolemma integrity. *J. Cell Biol.* 200:523–536. http://dx.doi.org/10.1083/jcb.201205118

Rivière, C., O. Danos, and A.M. Douar. 2006. Long-term expression and repeated administration of AAV type 1, 2 and 5 vectors in skeletal muscle of immunocompetent adult mice. *Gene Ther.* 13:1300–1308. http://dx.doi.org/10.1038/sj.gt.3302766

Saffarian, S., E. Cocucci, and T. Kirchhausen. 2009. Distinct dynamics of endocytic clathrin-coated pits and coated plaques. *PLoS Biol.* 7:e1000191. http://dx.doi.org/10.1371/journal.pbio.1000191

Sanger, J.W., P. Chowrashi, N.C. Shaner, S. Spalthoff, J. Wang, N.L. Freeman, and J.M. Sanger. 2002. Myofibrillogenesis in skeletal muscle cells. *Clin. Orthop. Relat. Res.* 403(Suppl):S153–S162. http://dx.doi.org/10.1097/00003086-200210001-00018

Schafer, D.A., S.A. Weed, D. Binns, A.V. Karginov, J.T. Parsons, and J.A. Cooper. 2002. Dynamin 2 and cortactin regulate actin assembly and filament organization. *Curr. Biol.* 12:1852–1857. http://dx.doi.org/10.1016/S0960-9822(02)01228-9

Schook, W., S. Puszkin, W. Bloom, C. Ores, and S. Kochwa. 1979. Mechanochemical properties of brain clathrin: interactions with actin and alpha-actinin and polymerization into basketlike structures or filaments. *Proc. Natl. Acad. Sci. USA.* 76:116–120. http://dx.doi.org/10.1073/pnas.76.1.116

Shear, C.R., and R.J. Bloch. 1985. Vinculin in subsarcolemmal densities in chicken skeletal muscle: localization and relationship to intracellular and extracellular structures. *J. Cell Biol.* 101:240–256. http://dx.doi.org/10.1083/jcb.101.1.240

Sonnemann, K.J., D.P. Fitzsimons, J.R. Patel, Y. Liu, M.F. Schneider, R.L. Moss, and J.M. Ervasti. 2006. Cytoplasmic gamma-actin is not required for skeletal muscle development but its absence leads to a progressive myopathy. *Dev. Cell.* 11:387–397. http://dx.doi.org/10.1016/j.devcel.2006.07.001

Towler, M.C., P.A. Gleeson, S. Hoshino, P. Rahkila, V. Manalo, N. Ohkoshi, C. Ordahl, R.G. Parton, and F.M. Brodsky. 2004. Clathrin isoform CHC22, a component of neuromuscular and myotendinous junctions, binds sorting nexin 5 and has increased expression during myogenesis and muscle regeneration. *Mol. Biol. Cell.* 15:3181–3195. http://dx.doi.org/10.1091/mbc.E04-03-0249

Veiga, E., J.A. Guttman, M. Bonazzi, E. Boucrot, A. Toledo-Arana, A.E. Lin, J. Enninga, J. Pizarro-Cerdá, B.B. Finlay, T. Kirchhausen, and P. Cossart. 2007. Invasive and adherent bacterial pathogens co-Opt host clathrin for infection. *Cell Host Microbe.* 2:340–351. http://dx.doi.org/10.1016/j.chom.2007.10.001